DEPARTMENT OF PHYSICS
UNIVERSITY OF JYVÄSKYLÄ
RESEARCH REPORT No. 6/2008

THEORETICAL STUDIES OF ARTIFICIAL ATOMS AND LATTICES

BY

JUHA-PEKKA NIKKARILA

Academic Dissertation
for the Degree of
Doctor of Philosophy

To be presented, by permission of the
Faculty of Mathematics and Natural Sciences
of the University of Jyväskylä,
for public examination in Auditorium FYS-1 of the
University of Jyväskylä on September 5, 2008
at 12 o'clock noon

Jyväskylä, Finland
September 2008

Preface

This work has been carried out at the Department of Physics and at the Nanoscience Center of the University of Jyväskylä during the years 2006-2008.

I would like to thank my supervisor Professor Matti Manninen for clever and motivating guidance throughout this work. I would also like to thank Professor Stephanie Reimann and Doctor Matti Koskinen for fruitful co-operation. I am grateful to my present employer Inspecta LTD, and particularly to my current foreman Georg Bergström, because their patience and support have made it possible for me to accomplish this thesis.

The financial support of the Jenny and Antti Wihuri Foundation, and the Emil Aaltonen Foundation, are greatly acknowledged.

My greatest thanks go to my beloved ones, to my wife Laura and to my son Juuso for their support, and for filling my life with joy.

Jyväskylä, July 2008
Juha-Pekka Nikkarila

Abstract

In this thesis, I present a review of five publications that all in one way or another are related to low dimensional quantum systems. The thesis has three major areas, where in the first area I concentrate to quantum dots. In the second area, I discuss the relation of quantum liquids to quantum dots. Finally, I discuss quantum dot lattices and clusters, and their magnetic properties.

I go through the basic assumptions, computational methods, results and their interpretations of the semiclassical model I have used to describe quantum dots with few electrons. I show also that the physics of confined particle systems (in general) can be succesfully described with a generalized version of the model. I demonstrate that its range of usefulness is independent of the statistics of the confined particles by applying it to bosonic systems also. The role of the interparticle interaction seems also to be insignificant; the only thing needed is that *there is* an interparticle repulsion between particles. To prove this claim, I succesfully apply this model also to systems with Gaussian repulsion.

In this thesis, I will also consider the relation of quantum dots with quantum liquids. The composite fermion (CF) theory, originally developed to describe the physics of quantum Hall effect (QHE), has shown to be applicable also in describing quantum dots. I will go through some basic properties of that theory and go through a mathematical discussion related to that theory. The purpose of this was to prove mathematically that the wave functions of CF theory satisfy $\phi^{CF}_{\alpha,0,0} = \phi^{CF}_{0,\beta,1}$. Although I did not succeed with a complete proof, I observed it to be true in every case I succeeded to calculate.

In the last part, I review the physical properties of quantum dot lattices and clusters, and present the results of my own research. I go through the Hubbard and the Heisenberg models because they play a significant role in the calculations and analysis of my investigations. I found out that the (antiferro-)magnetic properties of 1D lattices with two p states per lattice site can be understood with corresponding antiferromagnetic Heisenberg model. Similar model can explain antiferromagnetism of many 2D and 3D clusters.

List of Publications

I J.-P. Nikkarila and M. Manninen, *Rotating electrons in quantum dots: Classical limit*, Solid State Commun. **141**, 209-213 (2007).

II M. Koskinen, S.M. Reimann, J.-P. Nikkarila and M. Manninen, *Spectral properties of rotating electrons in quantum dots and their relation to quantum Hall liquids*, J. Phys.: Condens. Matter, **19** 076211 (2007).

III J.-P. Nikkarila and M. Manninen, *Localization of particles in harmonic confinement: Effect of the interparticle interaction*, Phys. Rev. A **76**, 013622 (2007).

IV J.-P. Nikkarila, M. Koskinen, S.M. Reimann, and M. Manninen, *Magnetic phases of one-dimensional lattices with* 2 *to* 4 *fermions per site*, New J. Phys. **10**, (2008) 063013

V J.-P. Nikkarila, M. Koskinen, and M. Manninen, *Magnetism of quantum dot clusters: A Hubbard model study*, Eur. Phys. J. B **64**, 95-103 (2008)

The author has performed main part of numerical work in publications I, III, IV and V. and participated in few calculations of article II. He has written article III, and the drafts of papers I, IV and V, and participated in writing II. He has taken part in the derivation of the model used in the papers I and III.

Contents

Chapter 1

Introduction

1.1 Quantum mechanics in material physics

Quantum mechanics (QM) was developed and formulated in co-operation of several great physicists, and it has proven to be vigorous from its invention to present. The only problem on using it in material physics is that one can actually solve analytically hardly any macroscopic systems due to significant number of linked equations. Despite that, the triumphal march of quantum mechanics has kept on going. It was less than thirty years ago, when it was technically possible to confine electrons into two dimensions. This remarkable scientific breakthrough has initiated a new golden-age for theoretical condensed matter physics since it is much easier to handle theoretically particles in two dimension than in three dimension. An addition to that, artificial low dimensional systems have turned out to allow many interesting phenomena.

1.2 Quantum Hall Effect, a consequence for electrons confined to 2D

In 1980 German physicist Klaus von Klitzing found a new natural phenomenon, when he investigated properties of transistors at very low temperatures and high magnitudes of magnetic field. The accuracy of measurements was very good; the relative accuracy was about one per ten million. The results of his research were astonishing, he found a phenomenon that he named as a quantized Hall effect (QHE) as a distinction from the usual Hall effect. In the Figure 1.1 it is shown how the Hall resistance did not grow linearly as a function of magnetic field, instead of that it grew stepwise. [1]

Von Klitzing and his coworkers showed that the growth of the Hall resistance was step-like. The rise to the next step happened at very precise values of magnetic field. More interestingly, the value of Hall resistance R_H could be expressed as a function of natural constants

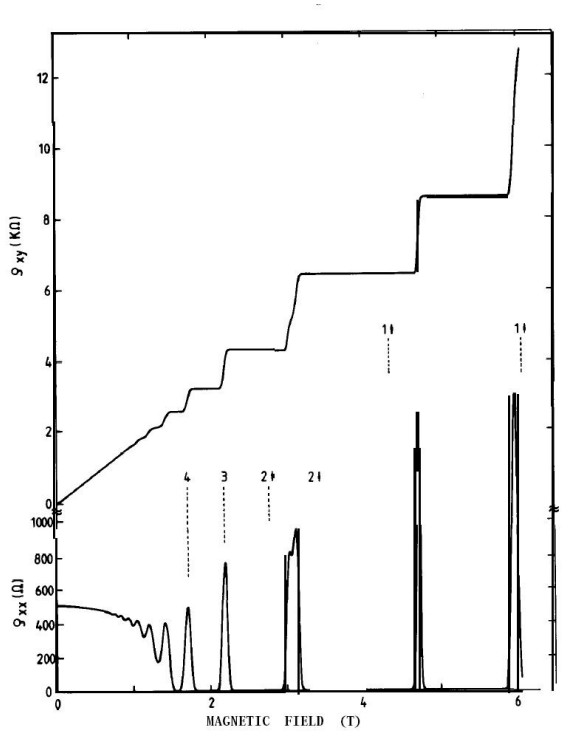

Figure 1.1: The main result of von Klitzing's measurements. The measurements were carried in 8mK temperature. The upper curve represents the behaviour of the Hall resistance $R_H \cong \rho_{xy}$, and the lower curve the diagonal part of the resistivity ρ_{xx}. (from Ref. [1])

$$R_H = \frac{h}{\nu e^2}, \tag{1.1}$$

where h is Planck's constant and e is elemental electric charge, and symbol ν is an integer number. The results were a surprise to the scientific community, because it was very unlikely that anything new was yet to be discovered in that field of physics. Von Klitzing was the first one to show that resistance, a macroscopic physical observable, was quantized. Later it is shown that at least specific heat capacity is also quantized. [2]

The scientific community held the von Klitzing's discovery very remarkable, and he was awarded the Nobel prize in physics already at 1985. Figure 1.1 is taken from von Klitzing's Nobel lecture, and one can observe that there occur risings on the Hall resistivity ρ_{xy} at very specific values of magnetic field. Another important observation is that there exists peaks on the diagonal resistivity ρ_{xx} at the same values of B. The phenomenon that Klaus von Klitzing observed is known currently as the integer quantum Hall effect (IQHE). It is used for example to measure very precisely the fine-structure constant (i.e. Sommerfeld fine-structure constant) $\alpha = \frac{e^2}{\hbar c}$. Furthermore, with the help of this phenomenon the unit of resistance Ω, can also be measured very accu-

rately. [3] Direct consequence for the accurate measuring of resistance is, that actually the unit Ω itself can be metrological defined with the help of QHE. [4, 5, 6, 7]

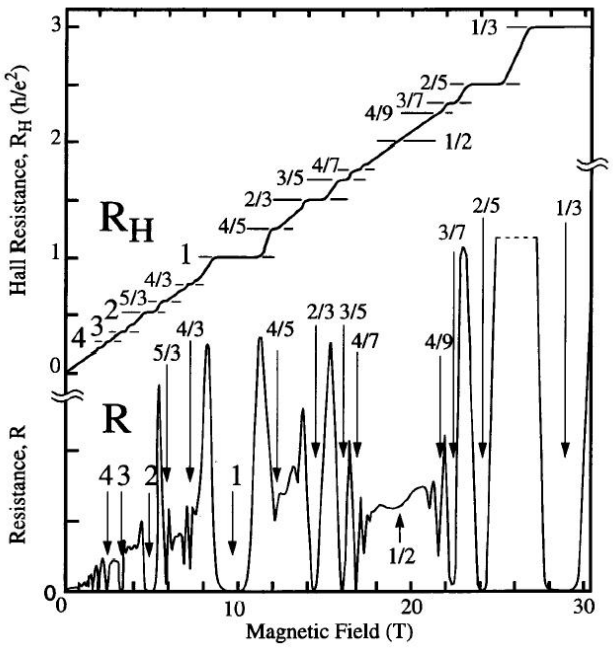

Figure 1.2: Horst L. Störmer and Daniel C. Tsui found that the Hall resistance had also values like $R_H = \frac{h}{\nu e^2}$, where ν is a common fraction and not an integer. First non-integer quantum Hall resistance value they observed was $\nu = 1/3$. In addition, Tsui and Störmer reported about minimum values in diagonal resistance R at the same points where the plateaus for R_H were observed. (from Ref. [8])

In 1982 German physicist Horst L. Störmer together with Chinese physicist Daniel C. Tsui, investigated this same phenomenon. They used even stronger magnetic fields and lower temperature. They first confirmed the results of von Klitzing, but furthermore, they found a new plateau in the Hall resistance. They noticed that if the value of resistance is expressed in the form (1.1), it equals very precisely the value for $\nu = 1/3$. Later they found more plateaus in the Hall resistance and showed that all of them can be expressed as in (1.1), if one accepts fractional values of ν. Tsui and Störmer were awarded the Nobel price in physics at 1998, and the phenomenon they found is known as the fractional quantum Hall effect (FQHE). [8]

Later it has been shown that the QHE is caused because of special quantum properties of electrons captured into two dimension. Capturing electrons into two dimensions was first done at the early 1980's. Russian physicist Alex Ekimov managed to capture electrons to a glass that contained also sulphur and lead. [9] The purpose of the measurements was basically to bound electrons to the plane, and thus to create a two-dimensional quantum dot (QD).

Just after these experiments, Russian physicists Efros and Efros published the first theoretical discussions concerning quantum dots. [10] A group working at Bell Laboratory, an American physicist Louis Brus leading it, investigated the properties of electrons with semiconductors. They managed to capture electrons in a very small region at plane. They noticed that energy spectrum of such group of electrons was discrete, reminding the properties of the electrons confined to an atom. Nowadays group of electrons confined to a small region is called as a quantum dot, or an artificial atom. The role of quantum dots in the future nanoelectronics is expected to be remarkable and their properties are examined in several universities throughout the world. [11, 12, 13]

1.3 Localization of particles into Wigner molecule

N electrons of a quantum dot can be set to rotation with the help of magnetic field. In the single-particle picture, the magnetic field puts every particle to rotate with some value l_j so that the total angular momentum is $L = \sum_{j=1}^{N} l_j$. If the magnetic field is strong enough, it polarizes the spins of the electrons. At large angular momenta the electrons also crystallize forming a rotating Wigner molecule. [14, 15, 16] The observation of localization raises up a question if the physics of a quantum dot could be understood using the means of classical physics.

The formation of a Wigner molecule is postulated in articles [I] and [III]. With that assumption we managed to show that spectral properties of a quantum dot at high angular momenta can be described with vibrational modes of the Wigner molecule. Furthermore, we showed that the exact form of the interaction of particles and the statistics of the particles are not critical on the formation of Wigner molecule. To be more specific, we demonstrated that the energetics of quantum dot can be understood with the help of classical physics regardless of what is considered to be the form of the interaction or the statistics of the particles. In research paper [II], I participated on calculation of a quantum dot with four and seven particles. The localization of particles into Wigner molecule was observed theoretically in that article. In articles [II] and [III], we showed that the localization of particles (when angular momentum is increased), is related closely to the expansion of the molecule. The expansion is initiated by the increase of centrifugal force. We showed that the width of the wave function of the particles remains unchanged, but the distances of the maxima are increased.

1.4 Magnetic properties of clusters and low dimensional lattices

More than a decade ago it was observed that clusters may exhibit stronger magnetic properties than corresponding bulk material. This kind of behavior has been reported for example for Iron, Nickel, Cobalt and for Gallium. [17, 18, 19, 20, 21] The experimentalists have been varying the cluster sizes extensively from few to few thousands of atoms. As usually in physics, interesting results of experiment have initiated an intensive theoretical phase, where for example the Hubbard model [22, 23], and different forms of the density functional theory (DFT), are applied. [24, 25, 26, 27] Eigenstates of single quantum dots with a few electrons can be calculated exactly by diagonalizing the many-body Hamiltonian (see Ref.[25] for review).

New experimental results have also been achieved in constructing artificial lattices from quantum dots. [28, 29, 30] Both lateral and vertical quantum lattices have been succesfully produced in experiments. Another example of artificial lattices are optical lattices – stable periodic arrays of potentials created by standing waves of laser light. [31, 32] The depths of the single traps may be changed with varying intensity of the laser light. By doing that, the experimentalists can confine ultra-cold atoms, of bosonic or fermionic character [33, 34, 35, 36, 37, 38], achieving particle numbers on the sites that may be even less than three. The strengths and the sign of the interparticle interactions between the atoms can be tuned by Feshbach resonances. [39, 40, 41, 42, 43, 44]

Also in theoretical analysis of artificial lattices, the usefulness of the density functional theory, has been shown. Mean-field calculations based on the spin-density functional theory predict that Hund's first rule orders the total spin of an individual (isolated) lattice site. [24, 25] Magnetic properties of the lattice itself depend on the total spin of the individual lattice sites, on the lattice structure and on the coupling between different lattice sites. [45, 46, 47, 48] Some of these findings can be understood with help of a simple tight binding model. [49] For calculating properties for quantum dot molecules, the density functional method has also been applied successfully. [50] Methods beyond the mean-field approximation have been applied also with quantum dot molecules. [51, 52, 53, 54, 55, 56]

The artificial and natural lattices have many differences. When the length scale in a normal lattice is significantly dependent on the strength of the interaction energy, an artificially made lattice can be nearly immune to this effect. The lattice structure itself is stable and the interactions of the particles are far too weak to break that ordering. This may lead to an internal symmetry breaking and, for example, to spontaneous magnetism, to superconductivity or even to superfluidity. New experimental results have lead to very rapidly developing theoretical epoch. [57, 58, 59, 60, 61, 62, 63, 38, 37] For the physics of a lattice with strongly correlated particles, the generic model is the Hubbard model, which has been intensively studied in the case of one state per lattice site (for reviews see [64, 65]). The simple Hubbard model is exactly solvable using the

Bethe ansatz.[66] Magnetism of finite molecules[22, 23] and quantum rings[67] have also been studied using the 1D Hubbard model.

1.5 About this thesis

In this thesis, I go through a review of five articles where I have contributed. An addition to those results, I present also some unpublished results that are mainly related to the composite fermion theory. In research papers [I] and [III], a semiclassical model was used on describing the physics (i.e. energetics and corresponding modes) of few particle quantum dots. It was shown that semiclassical model is appropriate in describing quantum dots with Coulombic and Gaussian inter-particle interaction. In those papers, we also showed that the particle statistics does not affect to validity of the model and it was demonstrated with bosonic particles.

In research paper [II], my main contribution was on calculation of energetics of quantum dots with four and seven particles. In that paper, the semiclassical model was used to demonstrate how the spin degree of freedom makes it possible that purely rotational state can be the lowest state of the system for every angular momenta. On that article, I also participated on calculation of overlap integrals (Table 3 in article [II]). With that table it was shown how well the exact diagonalization wave functions (with filling factors $\nu = 1/3$, $2/5$ and $2/3$, are overlapping with the Haldane-Halperin model wave functions.

In articles [IV] and [V], we considered Hubbard model in describing low dimensional quantum systems. In both articles, the exact diagonalization was used for solving the energetics of the systems. We concentrated on solving the spectral and magnetic properties of the systems on consideration. In both papers we analyzed results for half filling factor with a suitable Heisenberg model, which turned out to work in most of the cases. In article [IV], one-dimensional lattices were considered with two to four fermions per lattice site. In research report [V] we revealed the magnetic properties for various two and three dimensional clusters (triangle, tetrahedron, a row and a square with four lattice sites) with several orbitals (1s, 1p, 2s1d and even 1p with *three* p orbitals) per lattice site.

Chapter 2

Theoretical models and numerical tools

In this chapter a short introduction to theoretical models that are widely used to describe integer and fractional quantum Hall effects, is presented. These models are then expanded to describe quantum dots also. Laughlin theory and the next generation of it, the hierarchy theory are introduced first. They are followed by the composite fermion theory, which is proven to be very useful model with both versions of quantum Hall effect, and even with describing the physics of quantum dots, and graphene [68]. The Hubbard model, and the Heisenberg model, are in very intensive use on many fields of material physics. The exact diagonalization technique used in this thesis is presented in this chapter. We go through the eigenvalue problem both for a classical system and for a quantum mechanical system. Basically all energies and length scales in my research papers are presented in atomic units that are shortly introduced here as well.

2.1 Integral Quantum Hall Effect

American physicist Robert B. Laughlin revealed an explanation to IQHE already 1981. He showed that the phenomenon found by von Klitzing is a direct consequence of gauge invariance and the existence of a mobility gap (i.e. the quantization is derived by assuming the gauge invariance and a mobility gap). He proposed, that at very high magnetic fields the electrons nearby Landau levels cause the phenomenon (The Landau levels are discovered by Russian physicist Lev Landau). Landau levels represent the energy levels for a certain angular momentum (k vector). The lowest Landau level, for example, is defined to be the ground state energy for every angular momenta. In the same way, the second lowest Landau level is the group of second lowest energies for every angular momenta etc. Laughlin proposed that in phenomenon that von Klitzing found, all electrons are at the lowest Landau level. Qualitatively, the IQHE was

explained with a single particle picture. [69, 3]

2.2 Fractional Quantum Hall Effect

The phenomenon found by Tsui and Störmer, i.e. fractional quantum Hall effect (FQHE), was even more stunning than IQHE. IQHE could be understood as a phenomenon caused by electrons carrying charge e. If one used single particle picture in describing the physics of FQHE, the interpretation would be such that particles causing the phenomenon had charge that was a fraction of electron's charge, for example $e/3$. Only quarks are known particles that have charge that is a fraction of electron's charge. Therefore, single particle picture seemed to be rather poor approach in describing the physics of FQHE. [3, 70, 71]

2.3 Laughlin's theory

Year after the discovery of FQHE, first theoretical model was presented. The man behind this first model was American physicist Robert B. Laughlin. According to Laughlin, every successful theory should explain why the charge carriers seem to have charge that is a fraction of the electron's charge. He proposed that the electrons form together a many particle state that acts as a single particle. The state formed by the electrons he called **a quasiparticle** or **a quasielectron**, and its charge can be for example $e/3$. [3, 71]

Laughlin suggested that because the particles are bound into two dimension, one could choose a complex number $z_j = x_j + iy_j$ to represent the position of j^{th} particle. He also proposed that at a strong magnetic field the spins of the electrons are automatically polarized. Because of Pauli exclusion principle, the electrons resist compression strongly. They form a collective state, quantum liquid, which behavior can be described by one single wave function. Because of the Pauli exclusion principle, the quantum liquid is incompressible. It is also strongly correlated, which is due to the Pauli principle and the Coulomb repulsion. [3, 71]

The wave function must be antisymmetric in the interchange of particles, but it must also be an eigenstate of intrinsic angular momentum. Intrinsic angular momentum means that the center of mass angular momentum is omitted. Because the angular momentum L is conserved, the wave function must a polynomial with the coordinates $z_1, z_2, ..., z_N$, and with every term on the same order. The symbol N stands for number of particles. Laughlin noticed that the simplest wave function that fulfils these conditions is of the form

$$\Psi = \prod_{i<j}^{N} (z_i - z_j)^m e^{-\sum_{k=1}^{N} |z_k|^2}, \tag{2.1}$$

and it is an eigenstate of angular momentum with eigenvalue $L = N(N-1)m/2$. The wave function (2.1) is called nowadays as Laughlin wave function. The symbol m in the equation is an odd number and Laughlin showed that wave function describes a state where the Hall resistance (1.1) has a value that corresponds to factor $\nu = 1/m$. The model Laughlin presented could not explain the later found values for Hall resistance $\nu = 2/3$ or $\nu = 2/5$. Still, the theory proposed by Laughlin, and especially writing the wave function (2.1) has improved our knowledge of FQHE. Laughlin was awarded the Nobel Prize in physics with Tsui and Störmer in 1998. [3, 71]

2.4 Hierarchy Theory: Haldane-Halperin wave functions

The Laughlin theory have been extended afterwards to the hierarchy theory, where the quasiparticles form new quasiparticles. The formed state is in a way a "daughter" state of the initial quasistate. According to the hierarchy theory, for example a state corresponding to factor $\nu = 3/7$ is daughter state of $\nu = 2/5$ state, which itself is daughter state of a state corresponding to factor $\nu = 1/3$. The daughter state is followed from the parent state by adding to it *particle-like* or *hole-like* excitations. [72, 73, 3]

Maximum density droplet (MDD, i.e. a state with angular momentum $L = N(N-1)/2$), corresponds to a state with filling factor $\nu = 1$. Wave function for a given S_z is of the form

$$\Psi = \prod_{i<j}^{N/2+S_z} (z_i - z_j) \prod_{k<l}^{N/2-S_z} (\tilde{z}_k - \tilde{z}_l) \prod_{m,n} (z_m - \tilde{z}_n) e^{-\sum |z|^2}, \tag{2.2}$$

where the coordinates z_i label the positions of spin up particles and $\tilde{z}_i$ label the spin down coordinates. The Haldane-Halperin wave function represents a state with a non-simple fraction [72, 73]

$$\Psi_{\mathrm{HH}} = \prod_{i<j}^{N/2} (z_i - z_j)^q \prod_{k<l}^{N/2} (\tilde{z}_k - \tilde{z}_l)^q \prod_{m,n}^{N/2} (z_m - \tilde{z}_n)^p e^{-\sum |z|^2} \tag{2.3}$$

where q is an odd integer and p a positive integer that can be even or odd. One can notice that in the Equations (2.2) and (2.3), there exists also a spin degree of freedom. For example, the angular momenta $L = N(N-1)/2 + N^2/4$ and $L = 3N(N-1)/2 - N^2/4$ agree with the above wave function with $q = 1$, $p = 2$ and $q = 3$, $p = 2$, respectively. [II]

2.5 Composite Fermion Theory

Currently the generally used theory for describing FQHE is the composite fermion theory, which was published by Indian physicist J. K. Jain in 1989. He thought that the

hierarchy theory was not good enough in describing the physics of FQHE. According to Jain quasielectrons had too much peculiar properties, like fractional statistics. Moreover, the number of needed quasielectrons was far too large if one compared it to the number of normal electrons in that system. For example, the state corresponding to factor $\nu = 2/5$ arises from the state $\nu = 1/3$ when the number of quasielectrons would be about half of the number of normal electrons. According to Jain, the hierarchy theory did not present understanding of the microscopy of the phenomenon. Still, it gave a good classification for the states. [75, 76]

Hierarchy theory did not explain states, where the factor was on the form $\nu = p/q$ with even q. An example of states like that is a state with factor $\nu = 5/2$, which was discovered by Willet *et al* [74]. According to composite fermion theory, in principle all fractions are possible, but some are more stable than others. Jain wanted to reveal similarities between IQHE and FQHE, because difference on the origin of those two phenomena felt artificial. Jain wanted to explain these two phenomena with one single theory. [76]

On previous theories all particles were at the lowest Landau level (LLL). Jain thought that it was reasonable to allow particles to be also at the higher Landau levels. According to composite fermion theory, electrons form a collective state and the state itself acts like one particle. The wave function of this collective state is written as a function of electron coordinates in the same way as Laughlin wave function. As a distinction from Laughlin wave function, Jain wave function for FQHE is written with the help of any IQHE wave function. For example the state corresponding to factor $1/m$ is written as [76]

$$\Psi_{1/m} = \prod_{i<j}^{N} (z_i - z_j)^m e^{-\sum_{k=1}^{N} |z_k|^2} \, . \tag{2.4}$$

The above state is incompressible which can be seen by writing the wave function $\Psi_{1/m}$ with the help of wave function Ψ_1 corresponding to factor 1 [76]

$$\begin{aligned} \Psi_{1/m} &= \prod_{i<j}^{N} (z_i - z_j)^m e^{-\sum_{k=1}^{N} |z_k|^2} \\ &= \prod_{i<j}^{N} (z_i - z_j)^{m-1} \underbrace{\prod_{i<j}^{N} (z_i - z_j) e^{-\sum_{k=1}^{N} |z_k|^2}}_{=\Psi_1} \\ &= \prod_{i<j}^{N} (z_i - z_j)^{m-1} \Psi_1 \, . \end{aligned} \tag{2.5}$$

Jain's idea was that the Equation (2.5) can be interpreted so that electron unites with $m-1$ magnetic flux quanta and therefore carries flux $(m-1)\phi_0$ with it. Unifying magnetic flux quanta with electron does not destroy the incompressibility of the

original state since unification can be interpreted in mean field approximation so that a flux tube carrying flux $(m-1)\phi_0$ is attached to every electron. The flux tubes are not observables so attaching them with electrons do not destroy the correlations of the state Ψ_1 and therefore it stays incompressible. [75]

The result (2.5) can be generalized by formulating every FQHE wave function Ψ_ν with the help of IQHE wave function by attaching flux tube carrying magnetic flux $(m-1)\phi_0$ with every electron. Since the original state was incompressible, the resulting wave function is as well [76]

$$\Psi_\nu = \prod_{i<j}^{N}(z_i - z_j)^{m-1}\Psi_{\nu_1} \, . \tag{2.6}$$

The factor ν acquires then a form [76]

$$\nu = \frac{\nu_1}{(m-1)\nu_1 + 1} \, , \tag{2.7}$$

from which one sees that a FQHE state with factor ν has connected with an IQHE state with a factor ν_1. The trial wave function for FQHE is written by allowing the state to be partly at higher Landau levels. In summary, FQHE as a phenomenon is closely related to IQHE. In 1995 Jain proposed that also the physics of quantum dots can be expressed with the help of composite fermions. [75, 76, 77]

In practice, the composite fermion wave function for FQHE is derived by multiplying an IQHE wave function $(\phi_{m,n})$ with the Jastrow factor (2.8)

$$D^k = \prod_{i<j}(z_i - z_j)^{2k} \, , \tag{2.8}$$

and then projecting the result to Bargmann space, which represents LLL. It is physically reasonable to take a projection to the LLL, because the eigenenergies of the particles split into two parts when the magnetic field is increased. The confining part E_c of the energy is directly proportional to the magnetic field B, and it represents LLL. The interaction part V depends also on the magnetic field, but the dependency is weaker, $V \propto \sqrt{B}$. [77]

Projection to the LLL can be done in a general case, i.e. one can take a projection of an arbitrary holomorphic function ψ to Bargmann space. [82]

$$P\left(\psi\phi_{m,n}\right) = (-1)^{n+m} z^n \frac{d^m}{dz^m}\psi \, , \tag{2.9}$$

where n and m are positive integers. They determine the angular momentum and energy coordinates, although not directly, the (m,n) coordinate system is canted 45 degrees when compared to (L,E) coordinate system. The wave function of a non-interacting electron $\phi_{m,n}$ depends naturally only on one complex variable z. The result can be generalized to describe a system of several particles [82]

$$z^{\alpha} = z_1^{\alpha_1} \cdots z_N^{\alpha_N} \text{ and } \frac{\partial^{\beta}}{\partial z^{\beta}} = \frac{\partial^{|\beta|}}{\partial z_1^{\beta_1} \cdots \partial z_N^{\beta_N}} , \tag{2.10}$$

where indices α_i and β_i determine the angular momentum and energy coordinates of particle i and $|\beta| = \sum \beta_i$. In the Equation (2.10), we have introduced markings $\alpha = (\alpha_1, ...\alpha_N)$ and $\beta = (\beta_1, ...\beta_N)$. We notice that the (α, β) coordinate system is canted by 45 degrees when compared to (L, E) coordinate system, as is seen in Figure 2.1.

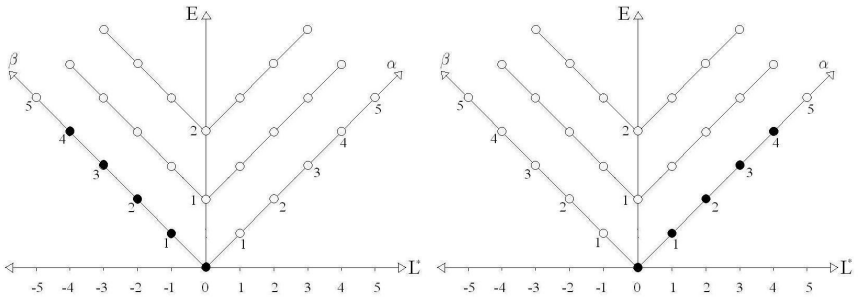

Figure 2.1: Left panel: a five-particle system at the ground state for angular momentum $L = -10$. Right panel: a five particle system at the ground state for angular momentum $L = 10$. In both cases, black dots represent particles, i.e. one particle in the system has this particular angular momentum and energy (L, E) combination. The combination can also be presented in the coordinate system (α, β). In both systems the particles are non-interacting particles.

The composite fermion wave function for N particle system is an antisymmetric product of one particle wave functions [82]

$$\phi^{CF}_{\alpha,\beta,k} = A[z^{\alpha}(\frac{d^{\beta}}{dz^{\beta}} D^k)]e^{-\frac{1}{2}|z|^2} , \tag{2.11}$$

where $\exp(-|z|^2/2)$ is the ground state wave function of harmonic oscillator, and A is an antisymmetric operator that is explained in more detail below. In practise, the antisymmetric operator antisymmetrizes the single particle states with respect of all α_i and β_j. The wave function (2.11) represents interacting electrons forming a quantum dot with angular momentum L [77]

$$L = L^* + kN(N-1) , \tag{2.12}$$

where L^* is angular momentum for corresponding non-interacting system. The angular momentum L^* for a quantum dot formed with non-interacting particles is bounded between values

$$-\frac{N(N-1)}{2} \leq L^* \leq \frac{N(N-1)}{2} . \tag{2.13}$$

The composite fermion theory basically represents a system of interacting particles rotating with angular momentum L with the help of a system of noninteracting particles rotating with angular momentum L^*.

From Figure 2.1 we see that the ground state of noninteracting particles in positive angular momentum L^* is mirror symmetric in E-axis with a ground state of negative angular momentum L^*.

In the Equation (2.11), there occurs an operator A that creates an antisymmetric product $A[\Psi]$. The operator A is on the form

$$A : \tau_0^p(\nu) \rightarrow \Lambda^p \nu \text{ so, that}$$
$$A[\Psi]\left(\tau_1, \tau_2, ..., \tau_p\right) = \frac{1}{p!} \sum_{\pi} \epsilon_\pi \Psi\left(\tau_{\pi(1)}, \tau_{\pi(2)}, ..., \tau_{\pi(p)}\right) , \tag{2.14}$$

where the sum is over all permutations $\pi = (\pi(1)\pi(2)...\pi(p))$ and $\epsilon_\pi = \epsilon_{\pi(1)\pi(2)...\pi(p)}$ is the Levi-Civita -number. An individual product $\Psi\left(\tau_{\pi(1)}, \tau_{\pi(2)}, ..., \tau_{\pi(p)}\right)$ is a product of variables τ_i forming a permutation $\left(\tau_{\pi(1)}, \tau_{\pi(2)}, ..., \tau_{\pi(p)}\right)$. If the permutation can be transformed into form $(12...p)$ with even number of hops, then $\epsilon_\pi = +1$, and if the same result is achieved with odd number of hops $\epsilon_\pi = -1$. The number $\pi(j)$ gives the j^{th} number, i.e. for permutation $(43...p)$ we get $\pi(1) = 4$ and $\pi(2) = 3$.

2.6 Diagonalization of quantum mechanical Hamiltonian using Configuration Interaction (CI) method

Hamiltonian for a quantum dot is of the form

$$H = \sum_{i=1}^{N} \left(\frac{\mathbf{p}_i^2}{2m} + V_{\text{ext}}(\mathbf{r}_i) \right) + \sum_{i<j}^{N} V(\mathbf{r}_i - \mathbf{r}_j) , \tag{2.15}$$

where $V_{\text{ext}}(\mathbf{r}_i)$ stands for external potential. In practice, external potential is often two-dimensional harmonic potential. The form for kinetic energy is familiar, and we have used two different potentials to describe the interparticle interaction. In papers [I-III], we used the usual Coulombic repulsion

$$V(r) = \frac{e^2}{4\pi\varepsilon\varepsilon_0 r} \tag{2.16}$$

to describe the interparticle interaction. In research [III], also Gaussian-type repulsion

$$V(r) = \frac{1}{\pi\sigma^2} e^{-r^2/\sigma^2} \tag{2.17}$$

was used to show that the semiclassical model presented in [I] is not sensitive to the shape of the interaction.

The eigenstates (and eigenenergies) of the Hamiltonian matrix (2.15) are solved using configuration interaction method. Let us assume that we have a complete N-electron basis set $\{\psi\}$. Any N-electron wave function may be written in a complete N-electron basis. The idea of the CI method is to write down the eigenvalue problem

$$H\Psi = E\Psi \tag{2.18}$$

and solve it by writing the eigenstate Ψ in a complete N electron basis $\{\psi\}$. Because the Slater determinants ψ_m form a complete basis, the wave function Ψ may be written as it follows

$$\Psi =: \Psi_{CI} = \sum_m C_m \psi_m \,, \tag{2.19}$$

where the coefficients C_m are to be solved.

An advantage of the CI method is that one can easily solve also the excitation energies and corresponding states. A disadvantage is that the calculations are very heavy, and the method is therefore not applicable to systems with more than about ten to fifteen particles. [78, 79]

It is convenient to use the occupation-number representation for Slater determinant. In that representation, a state corresponding to a certain particle configuration is written as

$$\psi = \big|001110000...\big\rangle \,. \tag{2.20}$$

Whenever a state is occupied (unoccupied), the number one (zero) is set to its place. The state on Equation (2.20) is written on the basis of the eigenfunctions of $2D$ harmonic oscillator. Furthermore, when one writes the state in that form one only takes into account the lowest Landau level. If one would take into account also the second Landau level, the state of Equation (2.20) was of the form

$$\psi = \left| \begin{array}{cccccccccccc} 0 & 0 & 0 & 0 & 0 & 0 & 0 & 0 & 0 & . & . & . \\ 0 & 0 & 1 & 1 & 1 & 0 & 0 & 0 & 0 & . & . & . \end{array} \right\rangle \,, \tag{2.21}$$

where the zeros at the second Landau level mean that it is not occupied. If the particle with highest angular momentum would jump into the second Landau level (and the angular momentum would conserve), the state would be

$$\psi = \left| \begin{array}{cccccccccccc} 0 & 0 & 0 & 0 & 1 & 0 & 0 & 0 & 0 & . & . & . \\ 0 & 0 & 1 & 1 & 0 & 0 & 0 & 0 & 0 & . & . & . \end{array} \right\rangle \,. \tag{2.22}$$

Let us write down the wave function corresponding to state (2.20) (or (2.21)) in Figure 2.2. From the picture we see that the angular momentum is $L = 2 + 3 + 4 = 9$. The right picture on Figure 2.2 shows a state showed in Equation (2.22).

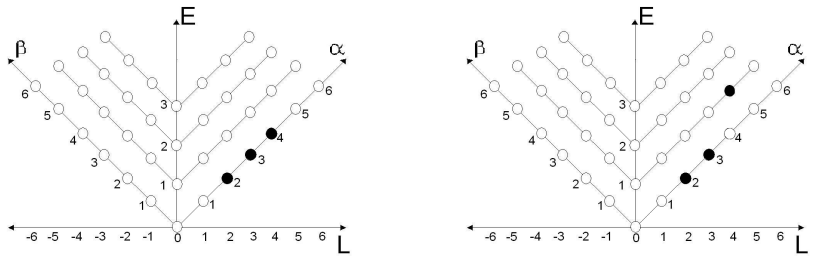

Figure 2.2: On left: A three-particle system at a state corresponding to angular momentum $L = 2 + 3 + 4 = 9$. One obtains that only the lowest Landau level is used. On right: A three-particle system in another state corresponding to angular momentum $L = 2 + 3 + 4 = 9$. One obtains that the particle on angular momentum 4 is at the second Landau level.

2.7 Diagonalization of the Hamiltonian for a classical few particle system: eigenenergies and corresponding eigenmodes

In the papers [I] and [III], we have considered classical (charged) particles confined to a harmonic potential. Lagrange mechanics is frequently used, when one has to solve a classical few particle system [80]. Lagrange mechanics is based on the Lagrangian function L

$$L = T - U, \tag{2.23}$$

where T is the kinetic energy of the system, and U is the potential energy of the system. By varying the time integral of the Lagrangian function (i.e. the action integral) in respect of $x_i(t)$, and finding the extremum (minimum, in practise) for the action, the Lagrangian equations of motion for x_i can be derived

$$\frac{\partial L}{\partial x_i} - \frac{d}{dt}\frac{\partial L}{\partial \dot{x}_i} = 0\,, \tag{2.24}$$

where $\dot{x_i}$ is a time derivative of variable x_i.

In present case we are interested in particles confined into two dimensions, solving the eigenfrequencies of the system, and then quantizing them. The goal is to see how well this kind of semiclassical model is describing the spectroscopy of quantum dots.

The eigenfrequencies ω for a system with linked equations of motion can be solved by finding the normal coordinates q_j and $\dot{q}_j$ for the system. With the help of the normal coordinates one can separate the Lagrangian into effective potential U_{eff}, which depends only on coordinates q_k, and into effective kinetic energy T_{eff} that depends only on coordinates $\dot{q}_k$ [80]

$$L = U_{\text{eff}}(q_1, ..., q_n) - T_{\text{eff}}(\dot{q}_1, ..., \dot{q}_1)\,. \tag{2.25}$$

The Lagrangian equation of motion (2.25) is simplified in such a way that

$$\frac{\partial U_{\text{eff}}}{\partial q_k} + \frac{d}{dt}\frac{\partial T_{\text{eff}}}{\partial \dot{q_k}} = 0\,. \tag{2.26}$$

If the equations of motion (2.26) are linear, their solutions are on the form $C_{1,k}\exp(i\omega t) + C_{2,k}\exp(-i\omega t)$. This can be written on matrix form and for both exponential form solutions separately. By skipping few intermediate steps, one comes to an equation

$$\begin{vmatrix} A_{11} - m_{11}\omega^2 & A_{12} & A_{13} & \dots \\ A_{21} & A_{22} - m_{22}\omega^2 & A_{23} & \dots \\ A_{31} & A_{32} & A_{33} - m_{33}\omega^2 & \dots \\ \vdots & \vdots & \vdots & \end{vmatrix} = 0\,, \tag{2.27}$$

where

$$A_{jk} = \frac{\partial^2 U_{\text{eff}}}{\partial q_k \partial q_j} \quad \text{and} \quad m_{jj} = \frac{\partial^2 T_{\text{eff}}}{\partial \dot{q}_j^2}\,. \tag{2.28}$$

Once the eigenenergies are solved, one has to find the corresponding eigenmodes. The symmetry properties of the eigenmodes are needed to define on which angular momenta they may be coupled to make a proper quantum state. We will handle the solution of eigenmodes more detail in the *Results* part, and in Appendix [C].

The problems considered next would be rather easy, if all the equations of motion were linear as we assumed when we derived the Equation (2.27). The problem is that when we take Coulombic (or Gaussian) form for interparticle interaction, the equations of motion are not linear. To solve this problem, one has to first linearize the equations of motion at their equilibrium position. Therefore, one has to first solve the classical equilibrium configuration of the system considered.

2.8 Quantization of classical vibrations and rotations

Previously the energy spectrum of a quantum dot has been discovered to be periodic as a function of the angular momentum L. [79] Our intention was to find out if the energy spectrum of a quantum dot could be reproduced from the energetics of corresponding classical system. Therefore, the methods for solving classical vibrations were considered in the previous section.

Once all the eigenmodes are solved, one has to quantize them. The quantization is performed as follows

$$\begin{aligned} \omega \rightarrow E_n &= \left(n + \frac{1}{2}\right)\hbar\omega \\ L \rightarrow L &= \hbar l\,, \end{aligned} \tag{2.29}$$

where $\hbar$ is the Planck constant and n a quantum number (an integer) telling the energy state of the harmonic oscillator. The symbol l is the quantum number for angular momentum L (and actually $L = L_z$ because the particles are confined into two dimension), and it is an integer.

The energy spectrum for a quantized system consists of quantized rotation energy and the vibration energy. The rotational energy E_{rot}, together with the interparticle interaction energy U_{inter} and the confining harmonic potential U_{harm} , determines the lowest possible energy value for certain angular momentum. This energy is therefore named as the classical zero-point energy E^0_{cl}, and it has an expression

$$E^0_{\text{cl}} = E_{\text{rot}} + U_{\text{inter}} + U_{harm} \, , \tag{2.30}$$

For symmetry reasons, this state can not be the lowest state energy for every angular momentum. The state has to be antisymmetric (symmetric) to be an acceptable state for a fermionic (bosonic) system.

The request of antisymmetric state leads to a selection rule, first derived by Maksym [14]

$$L + \sum_i n_i k_i = \begin{cases} 0 \text{ mod } p & \text{for } p = \text{odd} \\ p/2 \text{ mod } p & \text{for } p = \text{even}, \end{cases}$$

where the symbol p refers to the equilibrium geometry of the system (p-fold ring). The corresponding requirement for bosons is

$$L + \sum_i n_i k_i = 0 \text{ mod } p.$$

The symbols n_i refer to the number of excitations of mode ω_i and the number k_i to the symmetry property of the same mode (rotation by $2\pi k/p$ is presented by $\exp(i2\pi k/p)$).[14]

The energy spectrum of this semiclassical model is in general of the form

$$E_{\text{cl}} = E^0_{\text{cl}} + \sum_k \hbar\omega_k(n_k + \frac{1}{2}) + \hbar\omega_0(n_0 + 1), \tag{2.31}$$

where ω_k are all the vibration frequencies determined in the rotating frame and $n_k = 0,\ 1,\ 2, \cdots$. The last term corresponds to the center of mass excitations. In research report [I], the semiclassical energy spectrum for three and four electron systems is reported. In the article [III], a more general view of the problem was considered. In the latter report, first the semiclassical energy spectrum for seven electron system was revealed. In paper [III], also the semiclassical energy spectrum for three and four bosonic particles with Gaussian repulsion was studied.

2.9 Atomic units

All the numerical values presented in this thesis concerning the results of my papers are presented in atomic units. In the atomic unit system, one defines the units so that

$$e = m_e = \hbar = a_0 = 1\,, \tag{2.32}$$

which means that the charge and mass of electron (e and m_e), and the Planck constant and the Bohr radius ($\hbar$ and a_0) equal to one. The Bohr radius is on the form [81]

$$a_0 = \frac{4\pi\varepsilon_0\hbar^2}{m_e e^2}\,, \tag{2.33}$$

which leads immediately to a simplifying fact that in atomic unit system also

$$4\pi\varepsilon_0 = 1\,. \tag{2.34}$$

Let us consider an example to explain the numerics of atomic unit system. Electrons in a quantum dot can be considered to be confined in a harmonic trap. Let us assume the strength of the trap to be $\omega_0 = \frac{1}{2}$ (in atomic units). The corresponding strength for the spring constant k (in SI units) is

$$k = \omega_0^2 m_e = \frac{1}{4}\left(\frac{\hbar}{2\pi m_e a_0^4}\right)^2 m_e = \frac{\hbar^2}{16\pi^2 m_e a_0^2} \approx 10\frac{\mathrm{N}}{\mathrm{m}}, \tag{2.35}$$

a value that, interestingly, could also be a typical strength of a mesoscopic spring.

2.10 Generalized Hubbard model

The generalized Hubbard model Hamiltonian is on the form

$$\hat{H} = \hat{J} + \hat{U}, \tag{2.36}$$

where the first term represents the energy needed for hopping and the latter is the interaction energy. Hops preserve spin, and are equal for spin-up and spin-down particles. Thus, $\hat{J}$ separates into two symmetric spin parts: $\hat{J} = \sum_{\sigma=\uparrow,\downarrow} \hat{J}_\sigma$. Each part can be written as

$$\hat{J}_\sigma = -\sum_{nn'}\sum_{jj'} J_{nn'jj'}\left(c^\dagger_{njs}c_{n'j's} + h.c.\right), \tag{2.37}$$

where the index σ is the spin index, and n and n' refer to different dots (i.e. lattice sites). For every lattice site n, summation over n' includes all sites where the electron can hop from site n. When looking closer the expression for the hopping matrix (2.37), one notices that the generality of this model comes from the double summation over several states j and j' in each dot. In the usual Hubbard model, there is only one possible state (if the spin degree of freedom is excluded), where an electron can sit at one lattice site. The matrix element $J_{nn'jj'}$, in Equation (2.37), gives the energy scale

for electron to hop from its present state at (n, j) to an other state in (n', j'). In the article [IV], we considered lattices with one and two sub-atomic sites. In the research paper [V], we investigated clusters with two and three sub-atomic sites per one lattice site.

The interaction term in Equation (2.36) is approximated in the spirit of the tight-binding model: The particles interact only when they are at the same lattice site. Therefore, $\hat{U}$ separates in the symmetric parts representing interactions on each site n: $\hat{U} = \sum_n \hat{U}_n$. Within a site, full (spin-independent) two-body interaction is "allowed", which yields

$$\hat{U}_n = \frac{1}{2} \sum_{\substack{j_1 j_2 j_3 j_4 \\ \sigma\sigma'}} U_{j_1 j_2 j_3 j_4} c^\dagger_{n j_1 \sigma} c^\dagger_{n j_2 \sigma'} c_{n j_4 \sigma'} c_{n j_3 \sigma}. \tag{2.38}$$

Two-body interaction matrix elements $U_{j_1 j_2 j_3 j_4}$ are the direct space matrix elements of on-site interaction, depending on the interaction itself and the j-orbits in question, i.e. the eigenstates of the confining potential. Note that the total spin S and its z-component S_z are good quantum numbers. We diagonalize the system for $S_z = 0$ for even number of electrons and for $S_z = 1/2$ for odd number of electrons. The total spin S is determined after that for each many-particle state.

2.11 Heisenberg model

As mentioned in the Introduction part, earlier studies with artificial lattices have showed that Hund's first rule orders the total spin of an individual (isolated) lattice site. This has been observed by using mean-field calculations based on the spin-density functional theory. Furthermore, it is generally known that the simple Hubbard model at the limit of large U/t (U and t represent the interaction strength and the energy related to the hops, respectively) approaches the antiferromagnetic Heisenberg model. In research reports [IV] and [V], we have used the Heisenberg model in analyzing the results calculated with the Hubbard model. The effective Heisenberg Hamiltonian is on the form

$$\hat{H}_{\text{eff}} = \frac{1}{2} J_{\text{eff}} \sum_{n \neq n'}^{L} \mathbf{S}_n \cdot \mathbf{S}_{n'} + \text{constant}, \tag{2.39}$$

where $\mathbf{S}_n$ is the spin operator for site n. In the report [IV], we compare the Heisenberg and Hubbard models for the case of four sites, $L = 4$, where the spectrum of the antiferromagnetic Heisenberg model can be solved exactly[67, 84]. In the report [V], the corresponding comparison is made in all physical systems considered. In our research, the spin on Equation (2.39) can have values $1/2$, 1, or $3/2$ when first, second or third shell is half filled, respectively.

Chapter 3

Results

3.1 Semiclassical model in describing quantum dots

In this section, we present results that were published in papers [I], [II] and [III]. Maksym [85, 14] was the first one who tried to describe quantum dots with a semiclassical model. He showed that the lowest energy states for a few electron quantum dot can be explained with a reasonable simple model. We developed a comparable semiclassical model using a different technique to describe spectroscopic properties of quantum dots.

In publications [I] and [III], the equilibrium geometries of the systems considered were first revealed, and after that the solution for the eigenmodes was carried out by simply linearizing the equations of motion around the equilibrium position. After solving the eigenmodes (technique is shown in Appendix [C]), their symmetrical properties were solved by using group theory [86]. Finally, the energy spectrum of corresponding quantum dot was revealed. The quantum mechanical energies were determined via the following equation

$$E_{\rm cl} = E^0_{\rm cl} + \sum_k \hbar\omega_k(n_k + \frac{1}{2}) + \hbar\omega_0(n_0 + 1), \tag{3.1}$$

where ω_k are all the vibration frequencies determined in the rotating frame and $n_k = 0,\ 1,\ 2, \cdots$, and the last term corresponds to the center of mass excitations. The energy spectra for three and four electron quantum dots is presented in Figure 3.1 as open squares. The results in the figure show clearly that the energy spectrum can be understood well with this simple semiclassical model.

In paper [I], it was shown that both the whole low energy spectrum and the corresponding modes could be explained with a semiclassical model. The results of the first are shown in Figure 3.1, and the results for the latter are shown in Figure 3.2. The results indicate that, despite the many body theory is often needed to describe properly a quantum mechanical system, many properties, for example spectral properties, can indeed be explained with the help of this semiclassical model.

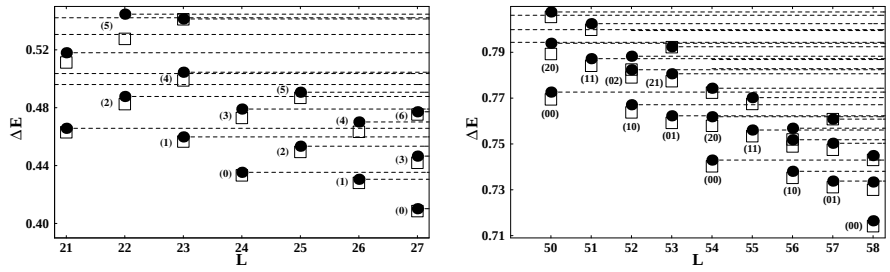

Figure 3.1: On the left: Many-particle energy spectrum for three electrons. The interaction energy is shown as a function of the angular momentum. The black dots are results of the Schrödinger equation and the open squares the results from the classical model. The center of mass excitations are not shown as points but are indicated as dashed lines. The numbers indicate the order of the vibration state a system of three noninteracting particles in its ground state (n_1). On the right: The same results for four electrons. The numbers indicate the vibration state (n_1, n_2).

These results are in accordance to observed localization of particles into a Wigner molecule [87, 88]. The localization is a necessary condition, but definitely not a sufficient, for manifestation of a classical model as an explanatory theory for quantum dots. Therefore, it was a little surprise that semiclassical model works so well as it does. Later, Fanga, *et al* [89] have found states that semiclassical model omits. On the other hand, Zhensheng Dai *et al* [90] have later published a fully quantum mechanical model that explains well the energetics and states of few particle quantum dots. In addition, the composite fermion theory has recently demonstrated, by Chuntai Shi *et al*, to explain properly the energetics and states of localized Wigner crystals (for which they used name 'CF crystals') [91].

We examined also how the semiclassical energy spectrum evolves on higher energy levels. Because of the mixing of the states, it is virtually impossible to directly compare the semiclassical and quantum energy spectra. Therefore, we concentrated to compare the density of states (DOS) from both spectra. By using DOS as a tool of research, we found that the similarity of these two spectra continues also at much higher energy levels than those shown in Figure 3.1.

In research paper [III], we continued to study semiclassical model. In that paper, we first showed that the energy spectrum for seven electrons could also be understood with the same semiclassical model used in [I]. The seven-particle-system was chosen because it has a very stable classical configuration: a hexagon with one electron at the center. The semiclassical and quantum mechanical spectra are presented in Figure 3.3, from which one can observe that the semiclassical model works well. Our result contradicts to the case of six electrons where Maksym *et al* [15] found two competing minima. They concluded that this competition spoils the explanatory value (in energy spectrum) of the semiclassical model. This is due to uncertainty of which classical equilibrium geometry will dominate in the energy spectrum.

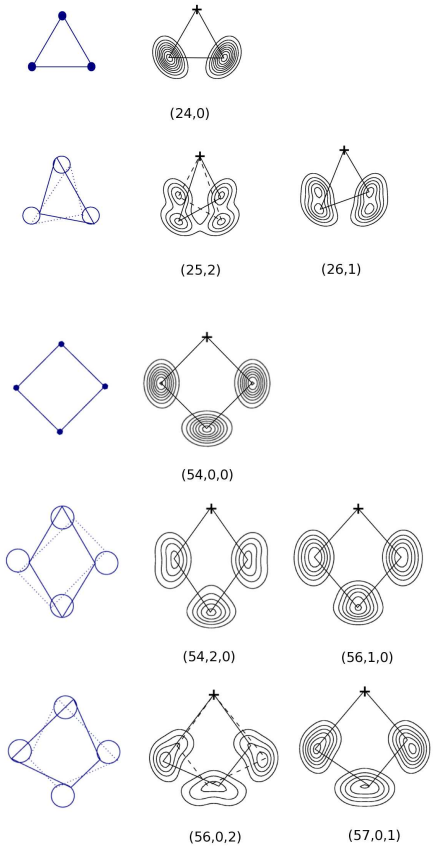

Figure 3.2: The left column shows the classical geometries and modes (pseudo-rotations) for three and four electrons. The two other columns show contour plots of the pair correlation functions from the quantum mechanical calculation. The reference point is shown as a cross. The relation of the pair correlation functions to the classical extreme geometries is indicated with solid and dashed lines. The numbers in parentheses are (L, n_1, n_2) indicate the angular momentum and the vibration state.

We found out that also with of seven electrons, other geometries than hexagonal are possible. Contradictory to the six-electron case, in the seven-electron case other geometries are much higher in energy. The picture on the left in Figure 3.4 is a non-vibrating state (pure rotational state), and it is drawn to illustrate a normal six-fold state. The picture on the right shows a state that is not six-fold but rather seven-fold, which is a quite interesting result as such. The state in the middle, on the other hand, is a normal excited state (but does not seem to be ashamed of it).

In the paper [III], we investigated also other interactions, and how they affect to the validity of the semiclassical model. We published some analytical results for harmonic repulsive interaction of the particles. The main results are derived in Appendix [A]. In addition, the Gaussian interaction was considered and investigated in the cases of three and four particle quantum dots as an example. Term “particle” was used because

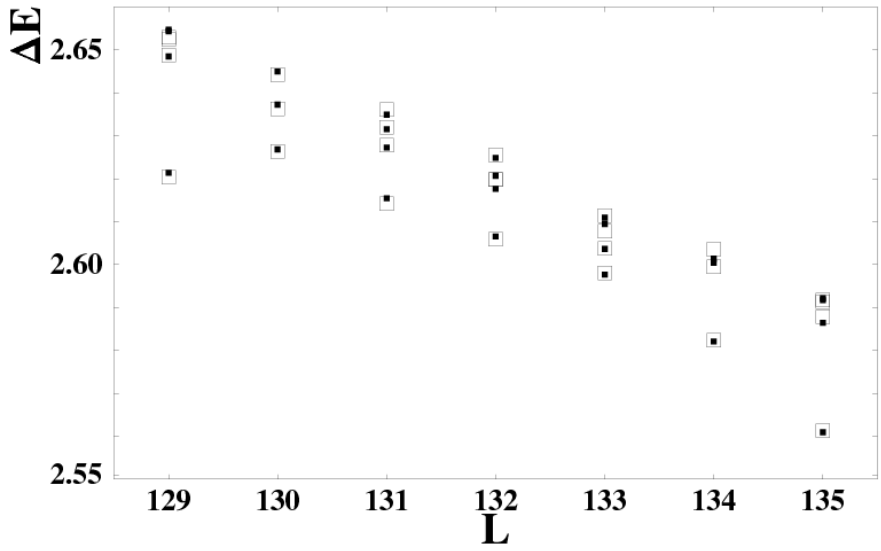

Figure 3.3: Low energy spectrum of seven electrons at high angular momenta. Black dots show the exact diagonalization results and open squares the results of the model Hamiltonian (8), shifted upwards with a constant 0.014. ΔE is the interaction energy in atomic units $\omega_0 = 0.5$. The ground states for $L = 129$ and 135 are purely rotational states. The ground states from $L = 130$ to $L = 134$ have vibration modes $\omega_5, \omega_4, \omega_6, \omega_7, \omega_3$, respectively.

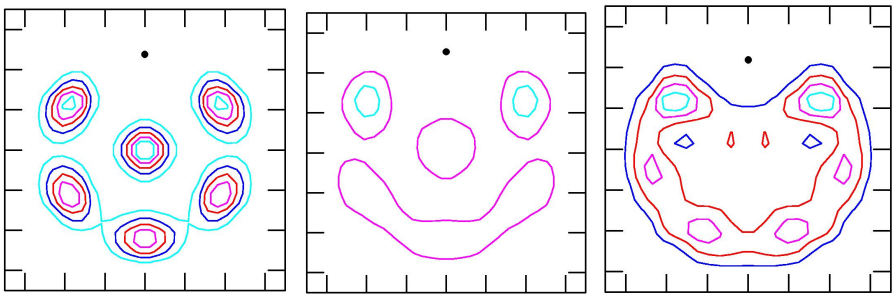

Figure 3.4: Pair correlation functions for selected states of seven electrons. Left panel shows the purely rotational state (ground state for $L = 117$). The center panel shows a vibration state (fourth excited state for $L = 133$), which consists of vibration modes ω_5 and ω_6. The right panel shows a seven-fold ring as a high-excited state (17th state for $L = 133$). The division between the frame ticks is 2 (in atomic units) and the reference point is shown as a black dot in each figure.

we investigated both fermions and bosons. The motivation for studying particles with Gaussian repulsion was that repulsive interaction between atoms can be approximated via such interaction. In the semiclassical model, it is essential to know which energy belongs to which mode. This fact leads to technical difficulties, because taking Gaussian repulsion to be the interparticle interaction, leads immediately to transcendent

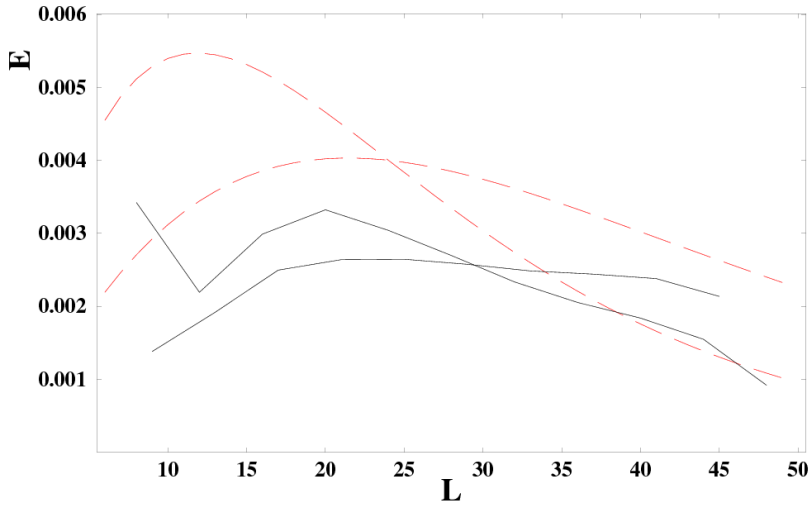

Figure 3.5: Dependence of the two low-energy vibration modes on the total angular momentum in the case of four fermions interacting with a Gaussian interaction with $\sigma = 3.0$. Dashed (red) lines show the classical results and solid black lines the quantum mechanical results from the exact diagonalization. All energies are in atomic units.

equations. Therefore, analytical results for the energies or their modes are not achievable. More importantly, keeping track on which energy belongs to which mode turns out to be somewhat challenging. With three electrons, the situation was easy because the number of relevant modes equals to one and it is easy to find.

With four particles, we had to solve numerically both the energies and the modes. It was necessary to find the right energy-mode pairs numerically, and this search had to be done for each angular momentum separately. Doing that was worthwhile, because I found out that the energies of the two lowest modes actually cross at certain L. If the semiclassical model explains the energetical properties of quantum dot properly, this state crossing should also happen in the quantum mechanical energy spectrum. That was exactly how it was. In Figure 3.5, we demonstrate the observed "phase transition" for both semiclassical and for quantum mechanical quantum dot. The "phase transition" is crystal clear on both case, although it does not occur at the same angular momentum.

Previously (see Ref. [25]) it has been noticed that the localization of particles in a quantum dot is related to angular momentum. Here we want to point out, that angular momentum does not seem to affect the electron probability distribution, which is demonstrated in Figure 3.6 (clearly, the variance W of the radius R for quantum ring considered, seems to stay constant even if the angular momentum L increases). When particles rotate with larger angular momentum, the localization occurs when the probability maxima of electrons move farther away from each other, which is illustrated in Figure 3.7. From that figure it is clearly seen that the magnitude of the angular

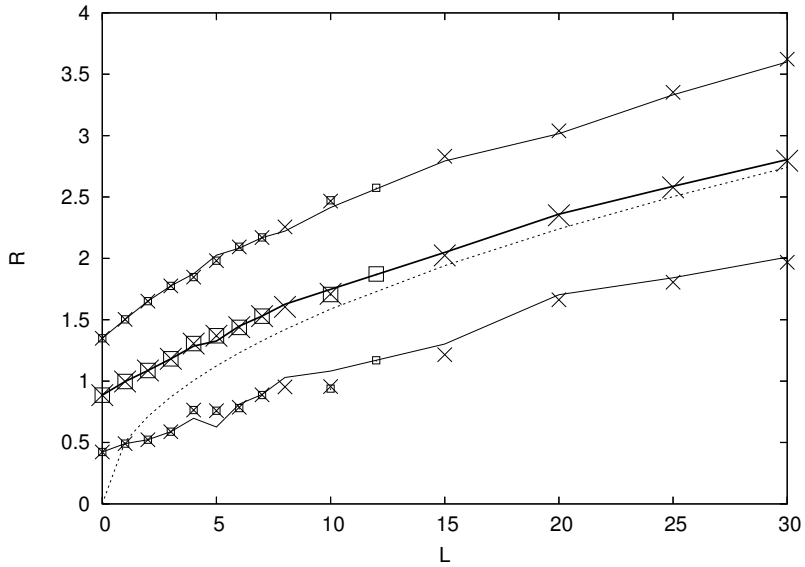

Figure 3.6: Average radius of the ring of four bosons as a function of the angular momentum L, calculated with exact diagonalization in the LLL. The centerline and -points show the radius R and the lower and upper lines and -points $R \pm W$. The variance of the radius is labeled as W. Solid lines show results for the Gaussian interaction with $\sigma = 3.0$, squares for $\sigma = 0.05$ and crosses for the Coulomb interaction. Dotted line is the result for classical particles with Gaussian interaction, $\sigma = 3.0$. The radii are presented in atomic units.

momentum does not have an effect to the probability distribution amplitude or to the width of the distribution.

We considered also rotational spectra of interacting particles in a 2D harmonic potential. In the 3D case, the classical particles interacting with repulsive interaction tend to form spherical shells. However, when put into rotation, it is energetically favorable for the 3D structure to collapse into a 2D structure due to the increased momentum of inertia. For a few particles, this happens already at small angular momenta.

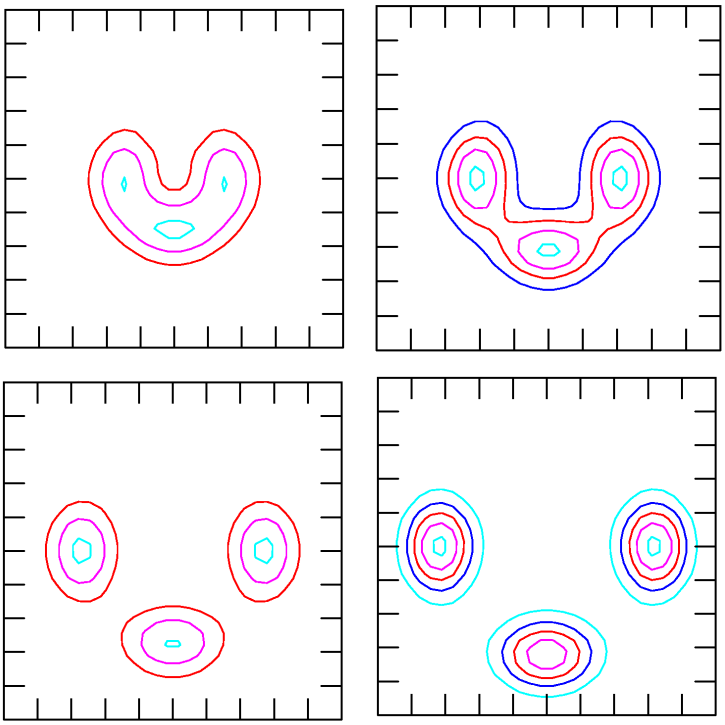

Figure 3.7: Pair correlation functions of four fermions interacting with the Gaussian interaction with $\sigma = 3.0$. Upper row shows results for $L = 10$ (left)and $L = 18$ (right) and the lower row for $L = 30$ (left) and $L = 42$ (right). The contour plots are in the same scale to demonstrate the expansion due to the rotation. The division between the frame ticks is 1 (in atomic units).

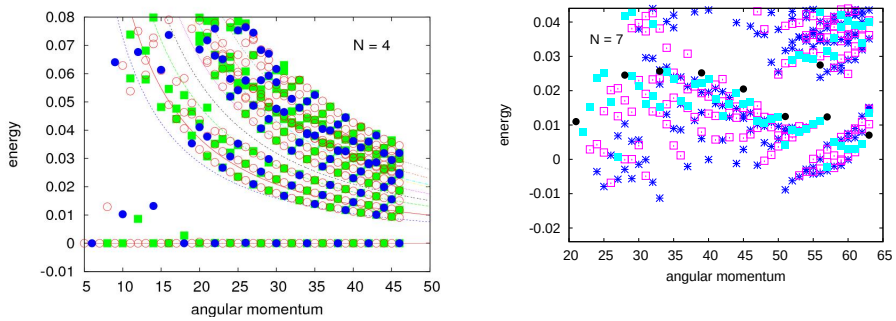

Figure 3.8: On the left: Excitation energies as a function of the angular momentum. Points are results of the exact diagonalization and the lines from the model of classical vibrations. Blue points: $S = 2$, open circles: $S = 1$, green squares: $S = 0$. On the right: Spectrum for 7 electrons $\nu = 1 \cdots 1/3$. Blue crosses: $S = 1/2$; blue squares: $S = 3/2$; red open squares: $S = 5/2$; black dots: $S = 7/2$. A third order polynomial fitted to the lowest energies has been subtracted from the total energy.

Table 3.1: Overlap between the exact result and the Halperin-Haldane model, $|\langle\Psi_{\rm HH}|\Psi\rangle|^2$, for different filling factors ν and electron numbers N

$N \setminus \nu$	1	$\frac{2}{3}$	$\frac{2}{5}$	$\frac{1}{3}$
2	1	1	1	1
3	1	.843	.920	.982
4	1	.636	.931	.958
5	1	.363	.911	.970
6	1	.162	.909	.980

Earlier [92] it has been shown that specific 3D structures collapse to 2D structure when are put to rotation. We studied the case of seven particles interacting with Coulomb interaction. We found that the ground state geometry of a non-rotating system is a pentagonal bipyramid, i.e. a five-fold ring in the x-y-plane with two atoms at positions $\pm c\hat{z}$. We also found that when such system is put to rotation, the five-fold ring expands while the particles in the z axis become closer to each other. The final phase transition from 3D to 2D structure occurs approximately at angular momentum $L = 7$. Similar results are obtained for other small particle numbers in 3D harmonic oscillator. Therefore, we concluded that the region where the classical model explains the spectrum for the 2D harmonic oscillator the result would be the same had we done the computations for the 3D confinement.

In research paper [II], my role was on computing energies of a quantum dot with four and seven particles. In that research, the semiclassical model was used with the spin degree of freedom. In Figure 3.8 excitation energies (on left panel) as a function of the angular momentum, are shown. The results show that the classical model with the spin degree of freedom explain all the lowest energies. In the figure (on right panel) spectrum for 7 electrons $\nu = 1 \cdots 1/3$, is presented. From that figure one observes a gap between the lowest band (purely rotational states) and the first excited band (lowest vibration states).

The spin degree of freedom makes it possible that purely rotational state can be lowest state of the system for every angular momenta. On article [II] also the symmetry of the order for states on both sides of angular momenta corresponding to filling fractions $\nu = 1/m$, with odd denominator, was observed (Figure 13 on article [II]). In that research, I also contributed on calculation of overlap integrals (Table 3 in article [II]). It was shown that the wave functions calculated by exact diagonalization (with filling factors , and), overlap with the Haldane-Halperin model wave functions well with $\nu = 1/3$ and reasonably well with $\nu = 2/5$ as shown in Table 3.1. From the table one observes that overlap is not so good when $\nu = 2/3$ and it becomes worse when the number of particles increases.

In conclusion, we have shown that at high angular momenta the energy spectrum of

particles confined to a 2D harmonic trap can be explained with the means of classical physics. The classical modes of localized particles were solved in a rotating frame of reference, and after that the modes were quantized. The form of inter-particle repulsion or the statistics that particles obey does not seem to affect to the localization or to the energy spectrum. It was pointed out that the situation would be the same for 3D harmonic trap, because the 3D structure collapses into 2D structure in any case, when the angular momentum increases. The validity of the semiclassical model in the presence of the spin degree of freedom was observed.

3.2 Composite Fermions

The composite fermion theory is widely used in describing the physics of quantum dots in addition to describing the nature of quantum Hall effect. My purpose was to show some mathematical properties of the composite fermion theory and use it to understood the systematics of the rotational spectra. However, we collided with several technical problems and therefore these results did not lead to publications. Nevertheless, we shortly go through some of my unpublished results in Appendix [B].

3.3 Magnetism in 1D quantum lattices, and in 2D and 3D clusters

In this section, we present results that were published in papers [IV] and [V]. We use generalized Hubbard model (2.36) to solve spectral and magnetic properties of quantum systems, mainly lattices and clusters. The strength of the interaction energy is used as a parameter in papers [IV] and [V]. In the previous research, we considered only δ potential to be the interaction energy, while in the latter paper we considered also Coulombic repulsion.

In the research paper [IV] we studied the magnetism of one-dimensional artificial lattices made of quasi-two-dimensional potential wells, for up to four particles per lattice site. In that region, the 1p level is (partially) filled. The 1s band was approximated to be filled completely, and only the 1p states were considered (shown in Figure 3.9). Numerical diagonalization of a generalized Hubbard model was performed for several particle numbers and filling fractions. The antiferromagnetic Heisenberg model was used in the analysis of the Hubbard model results.

An approximation is applied to the interparticle interactions with tight-binding interaction meaning that the interaction energy is finite only when the electrons are at the same lattice site. The ratio of interaction energy with electrons in the same state (e.g perpendicular-perpendicular) and interaction energy with electrons in different states (longitudinal-perpendicular) is approximated to be 3. Next, the validation of this approximation is presented.

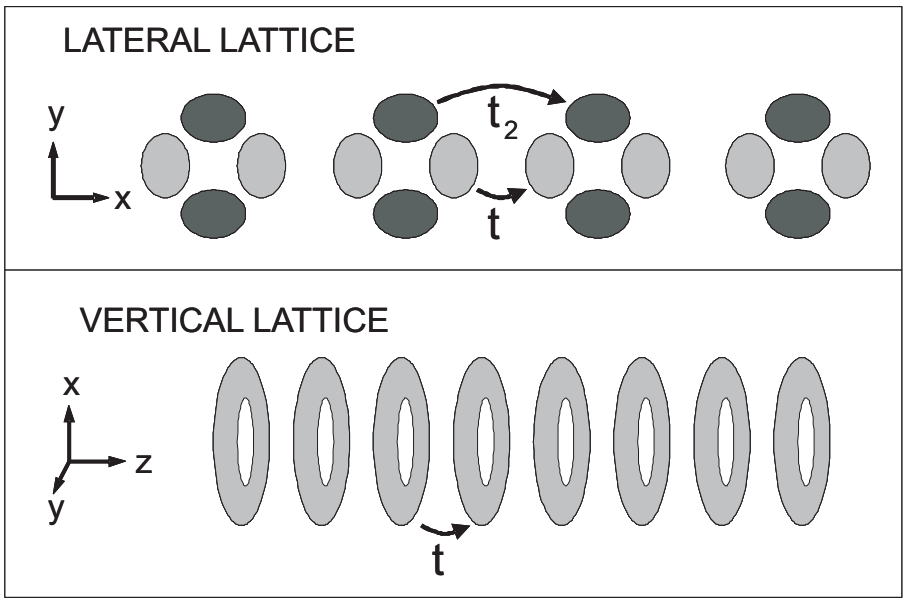

Figure 3.9: Schematic pictures of 1D lattices considered. Each lattice site has p_x and p_y orbitals. In the *lateral* case, these are shown as light and dark-gray densities. Here, the hopping probabilities t and t_2 between neighboring lattice sites are different for p_x and p_y orbitals. In the *vertical* case, it is natural to use states with 'rotating orbitals' p_{+1} and p_{-1} with circularly symmetric densities. In this case, there is only one hopping probability t.

Let us concentrate now on derivation of the earlier discussed relation for interaction matrix elements. We assume that the two states are p-states as they are in hydrogen atom

$$\begin{aligned} p_x &= xe^{-\alpha r} = r\cos\theta e^{-\alpha r} \\ p_y &= ye^{-\alpha r} = r\sin\theta e^{-\alpha r}\,, \end{aligned} \tag{3.2}$$

where (r,θ) are the electron's polar coordinates in 2D and (x,y) the corresponding Cartesian coordinates. We need to the matrix elements $\langle lm|V|pn\rangle$ for $\psi_l,\psi_m,\psi_n,\psi_p = p_x$ or p_y. Generally

$$\langle lm|V|pn\rangle = \int_{\mathbf{r},\mathbf{r}'} \psi_l^*(\mathbf{r})\psi_p(\mathbf{r})\psi_m^*(\mathbf{r}')\psi_n(\mathbf{r}')V(\mathbf{r}-\mathbf{r}'), \tag{3.3}$$

which is simplified after inserting in the delta interaction $V(\mathbf{r}-\mathbf{r}') = V_0\delta(\mathbf{r}-\mathbf{r}')$. The integration over $\mathbf{r}'$ can be performed

$$\langle lm|V|pn\rangle = V_0 \int_{\mathbf{r}} \psi_l^*(\mathbf{r})\psi_p(\mathbf{r})\psi_m^*(\mathbf{r})\psi_n(\mathbf{r}). \tag{3.4}$$

Because all the wave functions are proportional to $re^{-\alpha r}$, we get

$$\langle lm|V|pn\rangle = V_0 \int_{\theta=0}^{2\pi} f(\theta)d\theta \underbrace{\int_{r=0}^{\infty} \left(re^{-\alpha r}\right)^4 rdr}_{=A=\text{constant}}, \tag{3.5}$$

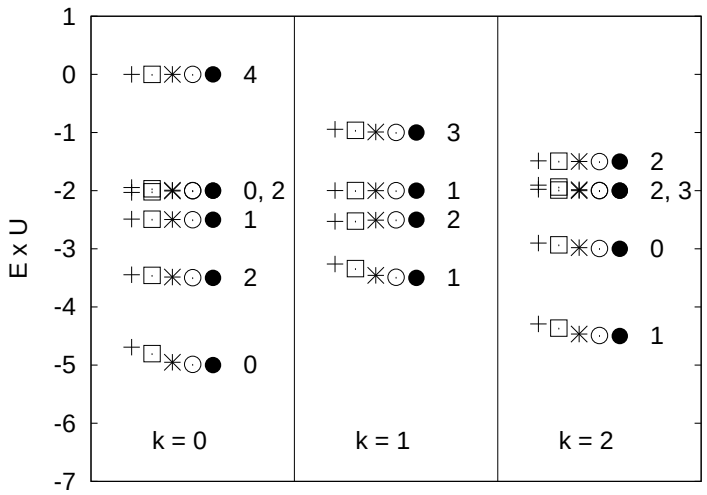

Figure 3.10: Lowest energy levels ($E \ll U$) for $L = 4$ and $N = 8$ calculated for different values of U. The numbers next to the levels denote the total spin S of the many-particle state. The wave vector k has values 0, 1, and 2. The symbols plus, square, star, circle and dot correspond to U values 2, 2.5, 5, 10, and 50, respectively. The energy levels for $U = 50$ agree with those of the $S = 1$ Heisenberg model with 0.01 % accuracy.

where $f(\theta)$ is a function that depends only on θ and it is determined immediately after the wave functions are chosen. The possible combinations for $f(\theta)$ are listed on the following

$$\begin{aligned}
&\cos^4\theta, \text{ for } \langle p_x p_x|V|p_x p_x\rangle \\
&\sin^4\theta, \text{ for } \langle p_y p_y|V|p_y p_y\rangle \\
&\sin^2\theta\cos^2\theta, \text{ if both } p_x \text{ and } p_y \text{ appear twice} \quad . \\
&\sin\theta\cos^3\theta, \text{ if } p_y(p_x) \text{ appears once (three times)} \\
&\sin^3\theta\cos\theta, \text{ if } p_x(p_y) \text{ appears once (three times)}
\end{aligned} \tag{3.6}$$

The integration in the expression (3.5) gives then $3\pi/4, 3\pi/4, \pi/4, 0, 0$, respectively. The ratio of the two different nonzero matrix is exactly 3. Even though we derived this relation for p-states that are for hydrogen-like potential $1/r$, it is true also for harmonic oscillator (HO) potential r^2, where the p-states are on the form $p_x = xe^{-\alpha r^2}$ and $p_y = ye^{-\alpha r^2}$. We denote the nonzero matrix elements as U and $3U$, in units of the hopping parameter t.

In the Figure 3.10 it is shown that in a vertical lattice, the system with half filling (and at the strong interaction limit) can be described correctly with the antiferromag-

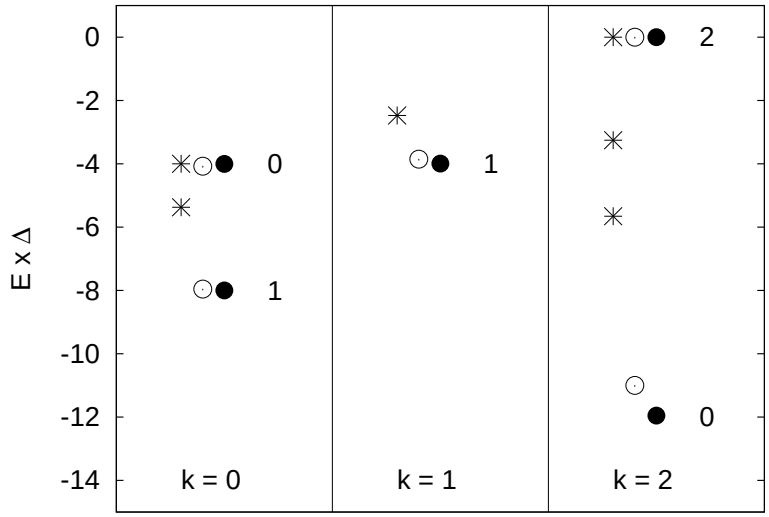

Figure 3.11: Lowest energy levels ($E \leq 0$) for polarized fermions with $L = 4$ and $N = 4$ calculated for different values of Δ for $U = 50$. The numbers next to the levels denote the total spin of the corresponding state of the spin-1/2 Heisenberg model. The wave vector k has values 0, 1, and 2. The symbols star, circle and dot correspond to Δ values 2, 10, and 50, respectively. The energy levels for $\Delta = 50$ agrees with those of the $S = 1/2$ Heisenberg model with 0.1 % accuracy.

netic Heisenberg model. Hubbard model results equal to Heisenberg model calculations within a 0.01% accuracy. It is emphasized that also at weaker interaction the computations show a qualitative similarity.

Results in the Figure 3.11, on the other hand, show an *orbital antiferromagnetism*. In that system, each site has two p states. The strong U limit in this case is an antiferromagnet where the 'magnetic moment' in each lattice site is not the spin but the orbital angular momentum of the p states, which can have the two values +1 or -1. The Heisenberg model energies equal to the Hubbard model energies within 0.1%.

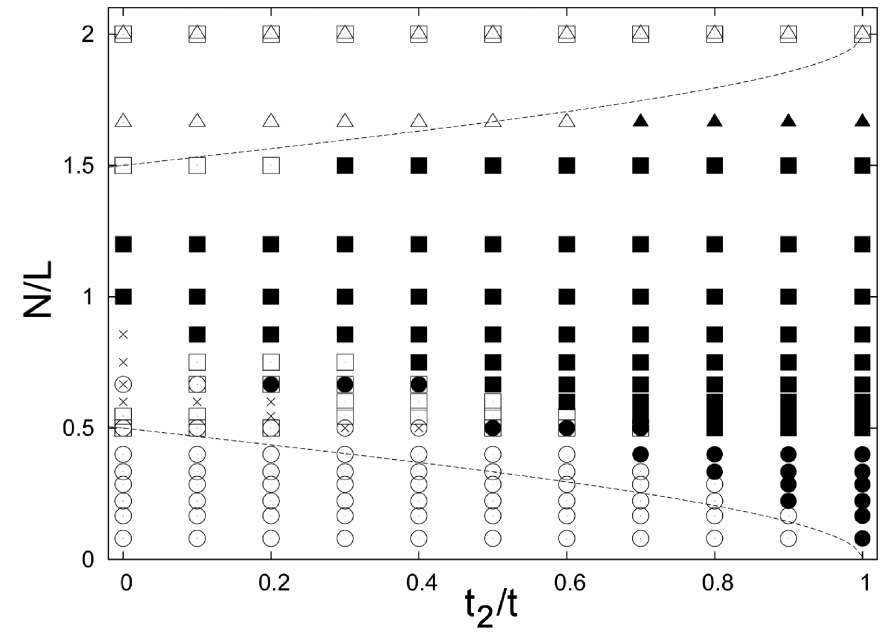

Figure 3.12: Magnetic phase diagram of the one-dimensional lateral lattice. The vertical axis shows the number of particles per site (on p-states) and the lateral axis the ratio t_2/t of the two hopping parameters. The dashed lines show the borders between which the narrower band (t_2 band) is filled. Outside this area the lattice is antiferromagnetic (except at $t_2 = t$). The filled (open) symbols show the ferromagnetic (antiferromagnetic) ground states obtained with exact diagonalization of the Hubbard Hamiltonian for 10 (triangles), 6 (squares), and 2 (circles) particles. Crosses show those results for $N = 6$, which are not ferro or antiferromagnetic, i.e. $0 < S < N/2$. The numerical results are for $U = 10$.

With lateral lattices, the whole magnetic phase diagram was resolved (Figure 3.12). Figure shows the magnetism of the lowest state as a function of both the number of particles per site (on the p-states) and the ratio t_2/t of the two hopping parameters. The limits shown in the figure are given by Eqs. (3.7)

$$\frac{N}{L} < \frac{1}{2\pi} \cos^{-1}(t_2/t) \; . \tag{3.7}$$

and (3.8)

$$N/L > 2 - \frac{1}{2\pi} \cos^{-1}(t_2/t) \tag{3.8}$$

and they are discussed in detail in article [IV]. One observes that between these limits, the ground state is mainly ferromagnetic, while outside these limits it is always antiferromagnetic. In the Figure 3.12, results for 2, 6 and 10 particles are shown. In the cases of $N = 4,\ 8,\ 12,\ \cdots$ the ferromagnetic state has a spin-wave (or domains) and interpretation of the magnetic structure is more difficult.

On the research [IV], it was found out that lattices seem to prefer ferromagnetism. An exception to that, in all systems under investigation, the half filled cases are anti-

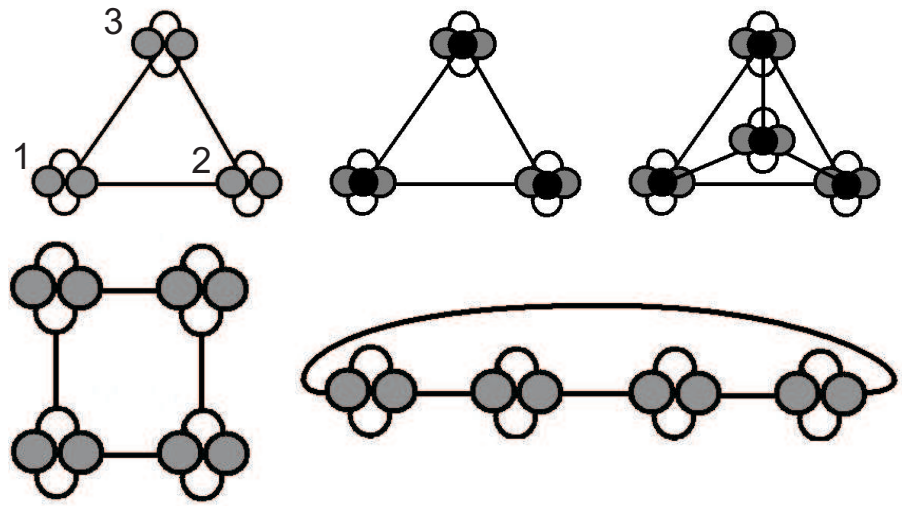

Figure 3.13: Schematic picture of clusters considered. Upper panel on the left: a triangle with orbitals p_x and p_y per lattice site; Upper panel on the middle: a triangle with orbitals p_x, p_y and p_z; Upper panel the right: a tetrahedron with orbitals p_x and p_y and p_z; Lower panel on the left: Four dots in a square; Lower panel on the right: Four dots in a row with periodic boundaries.

ferromagnetic and in those cases a corresponding antiferromagnetic Heisenberg model explained the results well.

In research report [V], several 2D and 3D clusters were considered. Their magnetic properties were revealed and in the cases of half filling factor they were interpreted with the help of a proper antiferromagnetic Heisenberg model. On the upper panel of the Figure 3.13, two triangle clusters and one tetrahedron cluster is presented. From left panel onwards the clusters are a triangle with two p states per site, a triangle with three p states per site and a tetrahedron with three p states per site, respectively. An addition to those, also a dimer was investigated, and four quantum dots (with partially filled p or sd shell) in a square and in a row. Schemadic pictures of considered four dot systems are presented on the lower panel of the Figure 3.13. The row geometry is presented with periodic boundaries, but also row geometry without periodic boundaries was investigated.

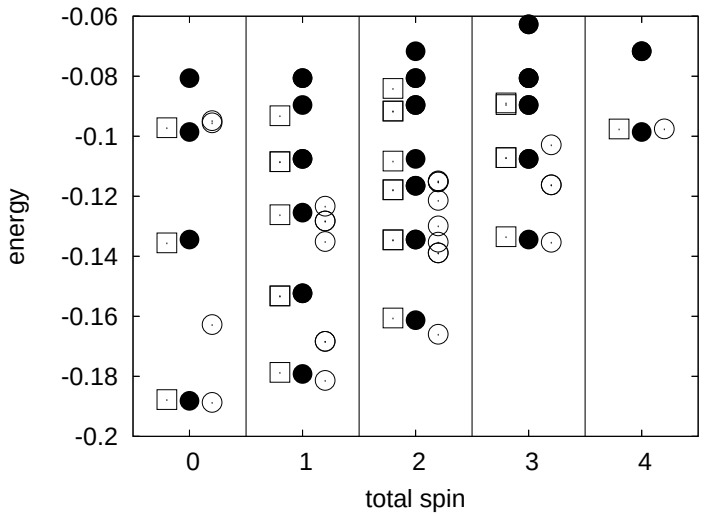

Figure 3.14: 25 lowest energy states for 12 sd electrons in a square calculated with the delta function ($U_{\max}/J_{\max} = 10$), squares, and with the Coulomb interaction ($U_{\max}/J_{\max} = 7.5$), open circles, compared with the results of the Heisenberg model, black dots. The results for the Coulomb interaction and the Heisenberg model have been scaled and shifted so that the ground state and the lowest $S = 4$ state agree with those of the delta function interaction.

It was found out that at the half filling of a dimer, a square and a row, a corresponding antiferromagnetic Heisenberg model can describe the spectroscopic and magnetic properties properly. The results for the square with half filled sd shells are presented in the Figure 3.14, and the same with row geometry is presented in the Figure 3.15. From the figures one observes that the spectrum calculated with the Hubbard model can be explained well with the help of corresponding Heisenberg model. A suitable Heisenberg model explained also the systems with half filled p orbitals.

The Heisenberg model turned out to describe well also triangular and tetrahedral quantum dot clusters at the half filling. We investigated only partially filled p orbitals for those clusters. The result was most evident with repulsive delta interaction but the agreement was good with the Coulomb interaction also. With tetrahedral geometry the dimension of the cluster was obviously three, and therefore three p orbitals per site was considered. With triangle geometry we investigated both two and three-dimensional clusters, i.e. two and three p orbitals, respectively. The results of triangular cluster showed that the only effect of the inclusion of the third p orbital, was to increase the spin per dot for the Heisenberg model.

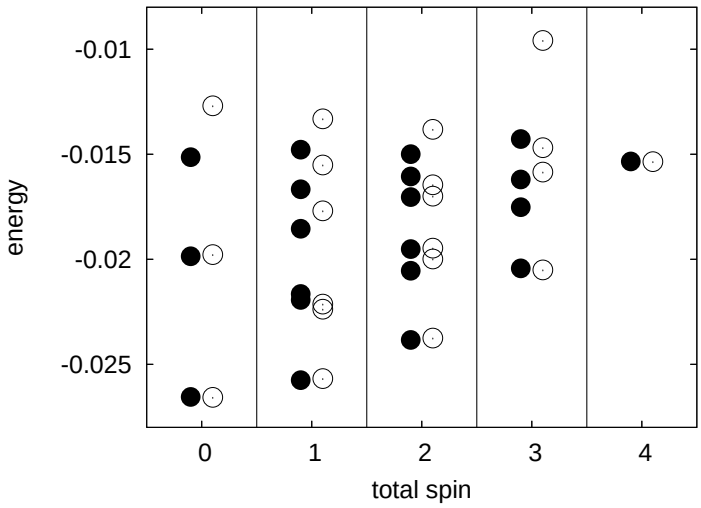

Figure 3.15: 25 lowest energy states for 12 sd electrons in a row of four quantum dots. Black points are results for a row of vertical dots calculated with the delta function interaction ($U_{\max}/J_{\max} = 40$), open circles are results for a row of lateral dots calculated with the Coulomb interaction ($U_{\max}/J_{\max} = 7.5$). The results for Coulomb interaction have been scaled and shifted so that the ground state and the lowest $S = 4$ state agree with those of the delta function interaction.

In the research papers [IV] and [V], we investigated 1D quantum dot lattice and several 2D and 3D quantum dot clusters. Three lowest shells $1s$, $1p$ and $2s1d$ were considered to be partially filled. Therefore, the generalized Hubbard model was used to solve the spectroscopic and magnetic properties of these systems. The antiferromagnetic Heisenberg model was used in the analysis of systems with half filled orbitals. The analysis showed that in all half filled cases the cluster or lattice is truely antiferromagnetic. With other fillings the considered systems favored mostly ferromagnetism.

Chapter 4

Conclusions

This thesis consists of five articles, which are related to three different subjects in material physics. Two of the articles handle quantum dots (papers [I] and [III]). In those publications, we consider a semiclassical model, whereby we tried to describe quantum dots. Article [II] covers an area of the relation of quantum liquids with quantum dots. Two of the articles are subjected to artificial lattices and artificial clusters that have multiple orbitals on their lattice sites (articles [IV] and [V]). In those articles, we made calculations with the Hubbard model and analyzed the results with a proper Heisenberg model.

In the first part (and articles [I] and [III]), we showed that the energy spectrum of interacting particles confined to a 2D harmonic trap can be explained with a semiclassical model. The classical vibration modes of localized particles were solved in a rotating frame of reference. Quantum mechanics was brought to the system by quantizing the energies of the modes and by using group theoretical means when combining the modes to the angular momentum. We managed to show that the form of interparticle repulsion or the statistics that particles obey makes no big difference to the validity of the semiclassical model. We went through a mathematical discussion related to composite fermion theory, but it did not lead to significant results.

In the research of quantum dot lattices and clusters (papers [IV] and [V]), We studied the magnetic phase diagrams for systems that consisted of artificial atoms with many particles. We found that majority of the systems favored ferromagnetism. However, In the cases where half of the states were filled, all the systems were antiferromagnets. In these cases, the antiferromagnetic Heisenberg model described well the low energy spectrum of the Hubbard model.

Appendix A

Harmonic interparticle repulsion

Here we consider a situation where there is, instead of the normal Coulombic repulsion, a repulsive harmonic interaction between particles. For two particles the total potential is then

$$U = \frac{1}{2}\left({\omega_0}^2\left({x_1}^2 + {y_1}^2 + {x_2}^2 + {y_2}^2\right) - \Omega^2\left((x_1 - x_2)^2 + (y_1 - y_2)^2\right)\right) \ , \quad \text{(A.1)}$$

where ω_0 is essentially the strength of the attractive harmonic interaction and Ω the strength of the repulsive harmonic interaction. The classical Hamiltonian matrix is

$$H = \begin{pmatrix} {\omega_0}^2 - \Omega^2 & \Omega^2 & 0 & 0 \\ \Omega^2 & {\omega_0}^2 - \Omega^2 & 0 & 0 \\ 0 & 0 & {\omega_0}^2 - \Omega^2 & \Omega^2 \\ 0 & 0 & \Omega^2 & {\omega_0}^2 - \Omega^2 \end{pmatrix} , \quad \text{(A.2)}$$

which is clearly block diagonal. Therefore, the displacements in the x and y directions can be treated separately.

By using simple algebra the eigenfrequencies can be solved

$$\begin{cases} \omega^2 = {\omega_0}^2 & \text{CM vibration, twofold degeneracy} \\ \omega^2 = {\omega_0}^2 - 2\Omega^2 & \text{twofold degeneracy} \end{cases} . \quad \text{(A.3)}$$

The eigenmode for the internal vibration is clearly of the form

$$\begin{cases} x = x_0 \sin \omega t \\ y = x_0 \cos \omega t \end{cases} . \quad \text{(A.4)}$$

Therefore the angular momentum is

$$L = I\omega = 2{x_0}^2\omega \,, \tag{A.5}$$

where x_0 is the x -coordinate of the equilibrium point and I stands for the moment of inertia. The total energy is

$$\begin{aligned} E =& \frac{L^2}{2I} + U_{\text{harm}} = \frac{4x_0^4\omega^2}{4{x_0}^2} + \left({\omega_0}^2 - 2\Omega^2\right){x_0}^2 \\ =& 2{x_0}^2\left({\omega_0}^2 - 2\Omega^2\right) \,. \end{aligned} \tag{A.6}$$

On the other hand, the system can be thought as a quantum mechanical harmonic oscillator that vibrates with frequency ω (neglecting the zero point energy)

$$E = n_1\omega = n_1\sqrt{{\omega_0}^2 - 2\Omega^2} \,, \tag{A.7}$$

where n_1 is the usual quantum number for vibration. By combining Equations (A.6) and (A.7) the equilibrium point can be expressed in a simple form

$${x_0}^2 = \frac{n_1}{2\omega} \,, \tag{A.8}$$

which leads to an important relation between the quantum numbers of rotation and vibration

$$L = 2{x_0}^2\omega = 2\frac{n_1}{2\omega}\omega = n_1 \,. \tag{A.9}$$

Now we can express the internal energy E_{int} in terms of angular momentum

$$E_{\text{int}} = E - L\omega_0 = L\left(\omega - \omega_0\right) \,, \tag{A.10}$$

from which we observe that the internal energy decreases linearly as angular momentum increases. It is an understandable result because the particles move farther apart from each others as the angular momentum increases.

It is easy to see that the eigenfrequencies in case of the harmonic interparticle repulsion are

$$\begin{cases} \omega^2 = {\omega_0}^2 & \text{CM vibration, twofold degeneracy} \\ \omega^2 = {\omega_0}^2 - n\Omega^2 & 2(n-1) \text{ -fold degeneracy} \end{cases} \,, \tag{A.11}$$

where n is the number of particles. We will now derive this result. The total potential energy for n particles is

$$U = \frac{1}{2}\left(\omega_0{}^2 \sum_{i=1}^{n}\left(x_i{}^2 + y_i{}^2\right) - \Omega^2 \sum_{i<j}^{n}\left((x_i - x_j)^2 + (y_i - y_j)^2\right)\right) , \qquad \text{(A.12)}$$

which leads to the classical $2n \times 2n$ Hamiltonian matrix that is clearly block diagonal. Therefore, the other part of the matrix can be dropped out, and the Hamiltonian is on the form

$$H = \begin{pmatrix} \omega_0{}^2 - (n-1)\Omega^2 & \Omega^2 & \Omega^2 & ... \\ \Omega^2 & \omega_0{}^2 - (n-1)\Omega^2 & \Omega^2 & ... \\ \Omega^2 & \Omega^2 & \omega_0{}^2 - (n-1)\Omega^2 & ... \\ \vdots & \vdots & \vdots & \end{pmatrix} , \qquad \text{(A.13)}$$

which is nxn matrix. The eigenvalue equation leads to the usual case, where the corresponding determinant D must vanish

$$D = \begin{vmatrix} \alpha & \beta & \beta & ... \\ \beta & \alpha & \beta & ... \\ \beta & \beta & \alpha & ... \\ \vdots & \vdots & \vdots & \end{vmatrix} = 0 , \qquad \text{(A.14)}$$

where the variables are

$$\begin{cases} \alpha & = \omega_0{}^2 - (n-1)\Omega^2 - \omega^2 \\ \beta & = \Omega^2 . \end{cases} \qquad \text{(A.15)}$$

The determinant D in the Equation (A.14) can be simplified by using general manipulation rules of determinant. If the first column is subtracted from every other column, the determinant remains invariant

$$D = \begin{vmatrix} \alpha & \beta - \alpha & \beta - \alpha & \beta - \alpha & ... \\ \beta & \alpha - \beta & 0 & 0 & ... \\ \beta & 0 & \alpha - \beta & 0 & ... \\ \beta & 0 & 0 & \alpha - \beta & ... \\ \vdots & \vdots & \vdots & \vdots & \end{vmatrix} , \qquad \text{(A.16)}$$

where all the off-diagonal values that are not in either in the first column or in the first row are zero. The determinant (A.16) can easily be expanded

$$\begin{aligned} D =& \alpha\left(\alpha-\beta\right)^{n-1} \\ & \underbrace{-\left(\beta-\alpha\right)\beta\left(\alpha-\beta\right)^{n-2}+\left(\beta-\alpha\right)\beta\left(\alpha-\beta\right)^{n-2}\cdot(-1)+...}_{=(n-1)\beta(\alpha-\beta)^{n-1}} . \\ =& \left(\alpha+\left(n-1\right)\beta\right)\left(\alpha-\beta\right)^{n-1} \end{aligned} \tag{A.17}$$

The determinant can now be inserted into the Equation (A.14). By taking the values for the constants α and β (A.15), we finally obtain Eq. (A.11). The $2(n-1)$ times degenerate internal vibration mode can also be solved easily. Let us consider only the movement in x -direction in which case we get

$$\begin{aligned} &\begin{pmatrix} {\omega_0}^2-\left(n-1\right)\Omega^2 & \Omega^2 & \Omega^2 & ... \\ \Omega^2 & {\omega_0}^2-\left(n-1\right)\Omega^2 & \Omega^2 & ... \\ \Omega^2 & \Omega^2 & {\omega_0}^2-\left(n-1\right)\Omega^2 & ... \\ \vdots & \vdots & \vdots & \end{pmatrix}\begin{pmatrix} x_1 \\ x_2 \\ x_3 \\ \vdots \end{pmatrix} . \\ &= \left({\omega_0}^2-n\Omega^2\right)\begin{pmatrix} x_1 \\ x_2 \\ x_3 \\ \vdots \end{pmatrix} \end{aligned} \tag{A.18}$$

Solving the matrix product leads to an equation group

$$\begin{cases} \left({\omega_0}^2-(n-1)\Omega^2\right)x_1+\Omega^2\left(x_2+x_3...+x_n\right) &= \left({\omega_0}^2-n\Omega^2\right)x_1 \\ \left({\omega_0}^2-(n-1)\Omega^2\right)x_2+\Omega^2\left(x_1+x_3...+x_n\right) &= \left({\omega_0}^2-n\Omega^2\right)x_2 \\ \vdots & \\ \left({\omega_0}^2-(n-1)\Omega^2\right)x_n+\Omega^2\left(x_1+x_2...+x_{n-1}\right) &= \left({\omega_0}^2-n\Omega^2\right)x_n \end{cases} . \tag{A.19}$$

This is actually the same equation appearing n times and it is true only if

$$\sum_{i=1}^{n} x_i = 0\,, \tag{A.20}$$

which means that the center of mass does not move. Therefore, the system can be put to vibrate in the simplest possible way that keeps the center of mass to stay at the origin. Two particles rotate at circular orbits while the rest remain still at the origin. Thus, the set of $2\left(n-1\right)$ times degenerate modes is on the form

$$\begin{aligned} \mathbf{X} = \{ &\left(\sin\omega t, -\sin\omega t, 0, ..., 0\right), \left(\sin\omega t, 0, -\sin\omega t, 0, ..., 0\right), ..., \\ &\left(\sin\omega t, 0, ..., 0, -\sin\omega t\right)\} \end{aligned} . \tag{A.21}$$

Appendix B

Results related to the CF theory

B.1 Symmetrics

The composite fermion wave function is on the form (2.11). The wave function has to describe fermions and consequently it has to be antisymmetric in every interchange of two particles. The antisymmetricity is achieved by using an antisymmetric product introduced in Equation (2.14). When $p = 3$, the antisymmetric product for particles (τ_1, τ_2, τ_3) is on the form

$$\begin{aligned} A[\tau_1,\tau_2,\tau_3] =& \frac{1}{3!}\Big(\epsilon_{123}A(\tau_1,\tau_2,\tau_3) + \epsilon_{213}A(\tau_2,\tau_1,\tau_3) + \epsilon_{132}A(\tau_1,\tau_3,\tau_2) \\ &+ \epsilon_{312}A(\tau_3,\tau_1,\tau_2) + \epsilon_{321}A(\tau_3,\tau_2,\tau_1) + \epsilon_{231}A(\tau_2,\tau_3,\tau_1)\Big) \\ =& \frac{1}{6}\Big(A(\tau_1,\tau_2,\tau_3) - A(\tau_2,\tau_1,\tau_3) - A(\tau_1,\tau_3,\tau_2) \\ &+ A(\tau_3,\tau_1,\tau_2) - A(\tau_3,\tau_2,\tau_1) + A(\tau_2,\tau_3,\tau_1)\Big) . \end{aligned}$$

As discussed before, a state of noninteracting many particle ground state with angular momentum $L^* = N(N-1)/2$ is mirror symmetric due energy axis with a ground state with angular momentum $L^* = -N(N-1)/2$.

B.2 Wavefunctions for positive angular momentum L^*

It can be seen from the form of composite fermion wave function (2.11), after tedious calculation, that for $k = 1$ and with positive L, the ground state has automatically a Slater determinant as a multiplier. The Slater determinant appears in Equation (2.8), where its power is 2. From the Figure 2.1 it is seen that when $k = 1$, which means that $\beta = (\beta_1, ...\beta_N) = (0, ..., 0)$, the derivatives do not occur in Equation (2.11). On the other hand, all permutations of numbers $0, ..., N-1$ appear in the antisymmetrization of $\alpha = (\alpha_1, ...\alpha_N)$. Therefore, all terms of the form $z_1^{\alpha_1}...z_N^{\alpha_N}$ appear in that equation.

The sign of one particular term $z_1^{\alpha_1}...z_N^{\alpha_N}$ is the same as the sign of the permutation itself. Later we notice that the Slater determinant is exactly what arises after going through these intermediate steps. The lowest energy eigenstate (for $k = 1$) is of the form

$$\begin{aligned}\phi^{CF}_{\alpha,0,1} =& \frac{1}{N!}\prod_{i<j}^{N}(z_i - z_j)\prod_{i<j}^{N}(z_i - z_j)^2 e^{-\frac{1}{2}|z|^2} \\ =& \frac{1}{N!}\prod_{i<j}^{N}(z_i - z_j)^3 e^{-\frac{1}{2}|z|^2} \ .\end{aligned} \tag{B.1}$$

Generally the wave function is of the form

$$\Psi^{CF}_{\alpha,0,k} = \frac{1}{N!}\prod_{i<j}^{N}(z_i - z_j)^{2k+1} e^{-\frac{1}{2}|z|^2} \ . \tag{B.2}$$

Clearly the wave function for positive angular momentum L^*, calculated starting from Equation (2.11) corresponds to composite fermion wave function for $L = (2k + 1)N(N-1)/2$, as it should.

The first part, i.e. the polynomial part of wave function (B.2) $\prod_{i<j}^{N}(z_i - z_j)^{2k+1}$ tells that the particles avoid each others. If two particles are at the same place, the wave function vanishes. It is notable that on increase in angular momentum (effectively k) makes this behavior even stronger. The other part $\exp(-\frac{1}{2}|z|^2)$ of the wave function prevents the particles to escape too far from the origin, because it approaches to zero faster than any possible polynomial approaches to infinity.

Next we will try to illustrate the probability function, which is the wave function (B.2), by drawing few schematic pictures. It is impossible to draw directly probability functions for two or more particle systems, because the degree of freedom is four or more, (and we can not draw four-dimensional pictures). The probability function for two particles

$$\phi^{CF}_{\alpha,0,k} = \frac{1}{2}(z_1 - z_2)^{2k+1} e^{-\frac{1}{2}(|z_1|^2+|z_2|^2),} \tag{B.3}$$

can be drawn with few tricks. In the two-particle case we can neglect the $y-$ coordinates, because the form of wave function (B.3) tells that the two particles are most likely at the same line with the origin. For three-particle system this is not the case, because actually it is seen from the wave function (B.2) that the particles tend to form an equilateral triangle with origin at the center.

The first trick is to assume that the particles are at the real axis. We still can not draw the probability function to plane because the degree of freedom is still two. However, we can now describe the one-dimensional system with two degrees of freedom as a two-dimensional system. In practice, the position of the first particle (in real axis) is

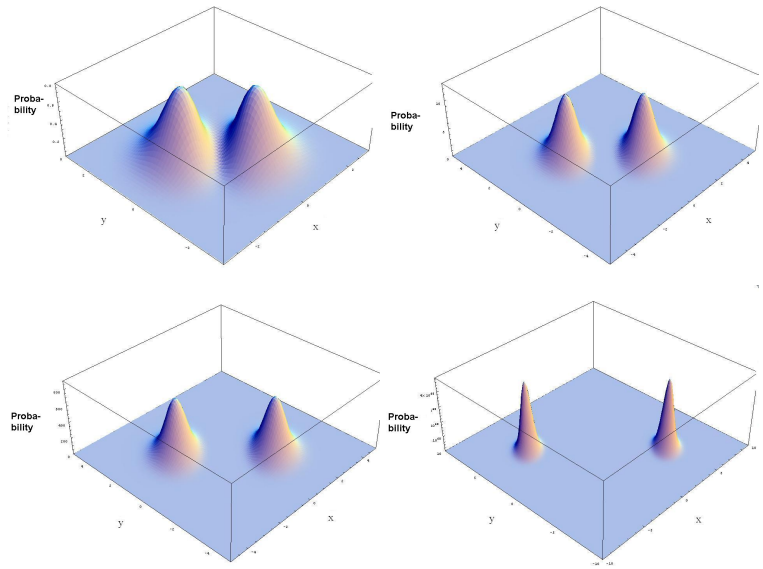

Figure B.1: On the left top corner: The probability of this figure can be understood so that its value in (X, Y) tells the probability of situation that the particles are in real axis at spots x and y. It is seen from the probability function that for angular momentum $L = 1$ two particles rotate very likely at directly opposite sites and in the same line with origin. On the right top corner: A two particle system rotating with angular momentum $L = 3$, i.e. $k = 1$. The probability function describes the physically trivial situation, where the particles rotate at the opposite sites from the rotational axis. On the left bottom corner: A two particle system rotating with angular momentum $L = 5$. On the right bottom corner: A two particle system rotating with angular momentum $L = 41$.

shown in x-axis, and the position of the other particle (that is actually also in the real axis) is shown in y-axis.

At the upper left corner in Figure B.1, there is shown a probability function of a two particle system with angular momentum $L = 1$, i.e $k = 0$. The particles rotate most likely at exactly on the opposite sites of the origin, because the peaks are highest at values $(x, -x)$ and $(-x, x)$. The probability function of two particle system rotating with angular momenta $L = 3$ ($k = 1$), $L = 5$ ($k = 2$) and $L = 41$ ($k = 20$) are also shown in Figure B.1. One can see from these pictures that the system indeed expands when angular momentum increases. The expansion is best shown in the system with angular momentum $L = 41$.

B.3 Wave functions for negative angular momentum L^*

One could assume that the wave functions should differ in situations where particles rotate align or against (and with the same value k) the direction favoured by the magnetic

field. Next we try to prove that they do differ, although they have some similarities, too. When the angular momentum is L, it can be easily seen that for positive and negative k values

$$\begin{aligned} L &= 2k_{\text{pos}} + 1 = 2k_{\text{neg}} - 1 \\ \Rightarrow k_{\text{pos}} &= k_{\text{neg}} - 1 \,. \end{aligned} \tag{B.4}$$

Therefore the wave functions should be related through an equation

$$\phi^{CF}_{\alpha,0,k} = \phi^{CF}_{0,\beta,k+1} \,. \tag{B.5}$$

We try to show the relation (B.5) between the wave functions for these cases. The wave function for negative angular momentum L^* with $k = 1$ should correspond to wave function for positive angular momentum with $k = 0$.

From the CF wave function one can see that when calculating the ground state for negative L^*, differentiating is the only mathematical operation that has to be performed for the antisymmetric product, multiplying with coordinates z is not executed. The differentiating is executed so that the number $\pi(j)$ in the Equation (2.14) (number β_j with markings of Equation (2.11)), tells how many times one has to differentiate with respect to coordinate j. For example, permutation $(43...p)$ means that the coordinate z_1 has to be differentiated four times, z_2 three times etc. In three-particle case with $k = 1$, the ground state for angular momentum $L = 3 \cdot (3-1) - 3 \cdot (3-1)/2 = 3$ is calculated as follows

$$\begin{aligned} \phi^{CF}_{0,\beta,1} = \frac{1}{3!}\Big(&\epsilon_{012}\frac{\partial^3 D}{\partial z_1^0 \partial z_2^1 \partial z_3^2} + \epsilon_{102}\frac{\partial^3 D}{\partial z_1^1 \partial z_2^0 \partial z_3^2} + \epsilon_{021}\frac{\partial^3 D}{\partial z_1^0 \partial z_2^2 \partial z_3^1} \\ &+\epsilon_{201}\frac{\partial^3 D}{\partial z_1^2 \partial z_2^0 \partial z_3^1} + \epsilon_{210}\frac{\partial^3 D}{\partial z_1^2 \partial z_2^1 \partial z_3^0} + \epsilon_{120}\frac{\partial^3 D}{\partial z_1^1 \partial z_2^2 \partial z_3^0}\Big) e^{-\frac{1}{2}|z|^2} \\ = -22 &\prod_{i<j}^{3}(z_i - z_j) e^{-\frac{1}{2}|z|^2} \,. \end{aligned} \tag{B.6}$$

The ground state wave function for negative angular momentum L^* in three particle case (B.6) differs from corresponding wave function (B.1) for positive angular momentum. On the other hand, the wave function (B.6) equals to wave function for L^*, when $k = 0$ (B.3).

The probability distribution for two-particle system rotating with angular momentum $L = 2 - 1 = 1$ is presented in Figure B.2. It seems that the negative angular momentum ground states for $k = 1$ are on the form

$$\phi^{CF}_{0,\beta,1} = C_N \prod_{i<j}^{N}(z_i - z_j) e^{-\frac{1}{2}|z|^2} \,, \tag{B.7}$$

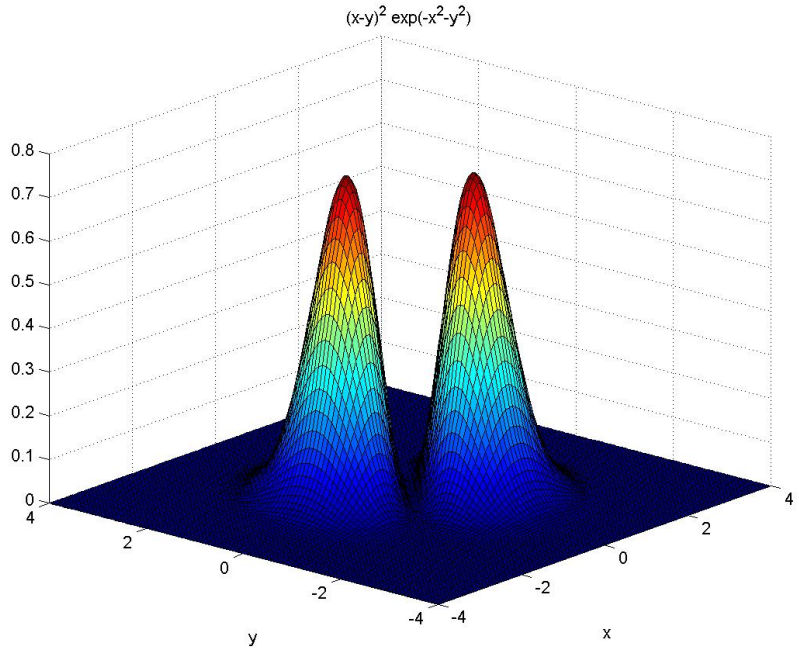

Figure B.2: Two-particle system rotates with angular momentum $L = 2\cdot(2-1)-2\cdot(2-1)/2 = 1$. The particles rotate very likely at the opposite sides of the rotation axis.

where C_N is a constant that depends on particle number N. If we could show that the Equation (B.7) is generally true, it showed that the composite fermion theory is at least in that case internally consistent. To show relation (B.7), we need only to show the antisymmetric derivative A_{der} for Jastrow factor (2.8) is generally on the form

$$A_{der} := A\Big[\frac{\partial^\beta D}{\partial z^\beta}\Big] = C_N \prod_{i<j}^{N}(z_i - z_j)\,, \tag{B.8}$$

when $k = 1$. The antisymmetrization goes through all the permutations $\beta = (\beta_1, ...\beta_N)$, where every number $0, ..., N$ appears exactly once. Let us write the Jastrow factor with the help of the sum of all these permutations

$$\begin{aligned} D &= \left((-1)^{\frac{N(N-1)}{2}} \sum_{\pi} \epsilon_\pi z^0_{\pi(1)} z^1_{\pi(2)} z^2_{\pi(3)} ... z^{N-1}_{\pi(N)}\right)^2 \\ &= \left(\sum_{\pi} \epsilon_\pi z^0_{\pi(1)} z^1_{\pi(2)} z^2_{\pi(3)} ... z^{N-1}_{\pi(N)}\right)^2 , \end{aligned} \tag{B.9}$$

where π stands for a certain permutation and ϵ_π tells its sign. Symbol $\pi(n)$ means the n^{th} permutation, and it gives the index for the complex number (i.e. $z_{\pi(n)}$). From the form (B.9) of the Jastrow factor one can see that two different complex numbers in

the same term cannot have the same degree. The degree of complex numbers in every term of the sum runs from zero to $N-1$. In the three particle case, the number of permutations is six, and the Jastrow factor as written in (B.9) is on the form

$$\begin{aligned} D &= \Big((-1)^{\frac{3*2}{2}}(z_1^0 z_2^1 z_3^2 - z_1^0 z_3^1 z_2^2 - z_2^0 z_1^1 z_3^2 + z_2^0 z_3^1 z_1^2 + z_3^0 z_1^1 z_2^2 - z_3^0 z_2^1 z_1^2)\Big)^2 \\ &= \big(z_2 z_3^2 - z_3 z_2^2 - z_1 z_3^2 + z_3 z_1^2 + z_1 z_2^2 - z_2 z_1^2\big)^2 \ . \end{aligned} \tag{B.10}$$

Let us now try to prove that the Equation (B.8) holds. We substitute the Jastrow factor (B.9) to the left side of Equation (B.8). In the next stage, there appears two independent sums over two permutations. By marking the permutations in the anti-symmetric product as β, and the permutations in the Jastrow factor as π, we get

$$\begin{aligned} A_{der} =& A\Big[\frac{\partial^\beta D}{\partial z^\beta}\Big] = A\Big[\partial^0_{z_1}\partial^1_{z_2}...\partial^{N-1}_{z_N}\Big(\frac{1}{N!}\sum_\pi \epsilon_\pi z^0_{\pi(1)} z^1_{\pi(2)}...z^{N-1}_{\pi(N)}\Big)^2\Big] \\ =& \frac{1}{N!}\sum_\beta \epsilon_\beta \partial^{\beta_1}_{z_1}\partial^{\beta_2}_{z_2}...\partial^{\beta_N}_{z_N}\Big(\sum_\pi \epsilon_\pi z^0_{\pi(1)} z^1_{\pi(2)}...z^{N-1}_{\pi(N)}\Big)^2 \ . \end{aligned} \tag{B.11}$$

From the Equation (B.11) one notices that the task would be a lot easier if the Jastrow factor were not powered to two. We could prove that the antisymmetric product is a constant:

$$\begin{aligned} & A\Big[\frac{\partial^\beta \prod_{i<j}(z_i - z_j)}{\partial z^\beta}\Big] \\ &= (-1)^{\frac{N(N-1)}{2}}\frac{1}{N!}\sum_\beta \epsilon_\beta \partial^{\beta_1}_{z_1}\partial^{\beta_2}_{z_2}...\partial^{\beta_N}_{z_N}\Big(\sum_\pi \epsilon_\pi z^0_{\pi(1)} z^1_{\pi(2)}...z^{N-1}_{\pi(N)}\Big) \\ &= (-1)^{\frac{N(N-1)}{2}}\frac{1}{N!}\sum_{\beta,\pi} \epsilon_\beta\epsilon_\pi \underbrace{\partial^{\beta_1}_{z_1}\partial^{\beta_2}_{z_2}...\partial^{\beta_N}_{z_N}\Big(\epsilon_\pi z^0_{\pi(1)} z^1_{\pi(2)}...z^{N-1}_{\pi(N)}\Big)}_{=\delta_{\beta,\pi}(N-1)!(N-2)!...(N-(N-2))!} \\ &= (-1)^{\frac{N(N-1)}{2}}\frac{(N-1)!(N-2)!...2!}{N!}\underbrace{\sum_{\beta,\pi}\delta_{\beta,\pi}\epsilon_\sigma\epsilon_\pi}_{\sum_\pi \epsilon_\pi^2 = N!} \\ &= (-1)^{\frac{N(N-1)}{2}}(N-1)!(N-2)!...2! \ . \end{aligned} \tag{B.12}$$

It is much more difficult to find a related equation for the actual wave function for negative angular momentum L^* (B.11). First, we notice that the number of terms increases rapidly because of the derivatives of the products. It is very difficult to see any regularity from these terms. It would be better to express the Jastrow factor as a one single sum to see more clearly the effects of the antisymmetric derivatives. Nevertheless, we can write the Jastrow factor as a multinomial [83]

$$(x_1 + x_2 + ... + x_r)^n = \sum_{n_1+...n_r=n} \binom{n}{n_1\,, n_2\,, ...\,, n_r} x_1^{n_1} x_2^{n_2} ... x_r^{n_r}\,, \tag{B.13}$$

where $\binom{n}{n_1\,,n_2\,,...\,,n_r} = \frac{n!}{n_1!n_2!...n_r!}$. For $k = 1$, the Jastrow factor (B.9) corresponds to the left side of multinomial (B.13). The sum over permutations is powered with two, so in the multinomial form $n = 2$. On the other hand, there is altogether as many terms as there is permutations π. Therefore $r = N!$ and the Jastrow factor is on the form

$$\begin{aligned} D = \prod_{i<j}(z_i - z_j)^2 &= \Big(\sum_{\pi} \epsilon_\pi z^0_{\pi(1)} z^1_{\pi(2)} ... z^{N-1}_{\pi(N)}\Big)^2 \\ &= \sum_{n_1+...+n_{N!}=2} \binom{2}{n_1\,, ...\,, n_{N!}} \Big(\epsilon_{\pi_1} z_1^{\pi_1(1)} ... z_N^{\pi_1(N)}\Big)^{n_1} ... \\ &\qquad ... \Big(\epsilon_{\pi_{N!}} z_1^{\pi_{N!}(1)} ... z_N^{\pi_{N!}(N)}\Big)^{n_{N!}}\,. \end{aligned} \tag{B.14}$$

The marking $n_1 + ... + n_{N!} = 2$ in the summation of Equation (B.14) means that the summing is performed over all strings $()$, where the sum of the indexes equals two. The summing (B.14) can be divided into two parts. There are altogether $N!$ terms in the first sum, where one of $n_1, ..., n_{N!}$ equals to two and the others are zero. In the second sum two of $n_1, ..., n_{N!}$ equal to one and the rest are zero. In the first sum, the factor $\binom{n}{n_1\,,n_2\,,...\,,n_{N!}} = 1$. We call this as the sum of diagonal terms, because in practice it is build by powering every term of the sum π and powering it to two, and then summing them. In the latter case, every term in the sum has a constant $\binom{n}{n_1\,,n_2\,,...\,,n_{N!}} = 2$ as a multiplier. This sum is called as the cross-term-sum, because it is build of terms where two cross terms of the sum π are multiplied. Then the Jastrow factor (2.8) reaches the form

$$\begin{aligned} D = \prod_{i<j}(z_i - z_j)^2 &= \Big(\sum_{\pi} \epsilon_\pi z^0_{\pi(1)} z^1_{\pi(2)} ... z^{N-1}_{\pi(N)}\Big)^2 \\ &= \underbrace{\sum_{\pi} z^0_{\pi(1)} z^2_{\pi(2)} ... z^{2(N-1)}_{\pi(N)}}_{\text{sum of diagonal terms}=:D_{\text{diag}}} \\ &\quad \underbrace{+\,2 \sum_{\pi_v \neq \pi_w} \epsilon_{\pi_v} \epsilon_{\pi_w} z_1^{\pi_v(1)+\pi_w(1)} z_2^{\pi_v(2)+\pi_w(2)} ... z_N^{\pi_v(N)+\pi_w(N)}}_{\text{sum of off-diagonal terms}=:D_{\text{cross}}}\,. \end{aligned} \tag{B.15}$$

The diagonal-term-sum behaves nicely in the antisymmetric derivative, which can be seen by inserting the Jastrow factor on the form (B.15) into Equation (B.11)

$$\begin{aligned} A_{der,\text{diag}} &= A\Big[\frac{\partial^\beta D_{\text{diag}}}{\partial z^\beta}\Big] \\ &= \frac{1}{N!} \sum_{\beta} \epsilon_\beta \partial_{z_1}^{\beta_1} \partial_{z_2}^{\beta_2} ... \partial_{z_N}^{\beta_N} \Big(\sum_{\pi} z^0_{\pi(1)} z^2_{\pi(2)} ... z^{2(N-1)}_{\pi(N)}\Big)\,. \end{aligned} \tag{B.16}$$

After antisymmetric summation only derivatives of the form

$$\begin{aligned}
&\partial^0_{z_1}\partial^1_{z_2}...\partial^{N-1}_{z_N}(z_1^0 z_2^2...z_N^{2(N-1)}) \\
&= \Big(2(N-1)[\overbrace{2(N-1)-1}^{=2N-3}]...[\overbrace{2(N-1)-(N-2)}^{=N}]\Big)\cdot \\
&\Big(2(N-2)[\overbrace{2(N-2)-1)}^{2N-5}]...[\overbrace{2(N-2)-(N-3)}^{=N-1}]\Big)\cdot ...\cdot \\
&\cdot\Big(2\overbrace{(N-(N-1))}^{=1}[\overbrace{2(N-(N-1))-1}^{=1}]z_1^0 z_2^1...z_N^{N-1}\Big) \\
&= 2^{N-1}(N-1)!\cdot\frac{1!}{1!}\cdot\frac{3!}{2!}\cdot ...\cdot\frac{(2N-5)!}{(N-2)!}\cdot\frac{(2N-3)!}{(N-1)!}z_1^0 z_2^1...z_N^{N-1}\ .
\end{aligned} \tag{B.17}$$

remain. It is worth of mentioning, that also following terms survive after taking the derivatives

$$\partial^0_{z_1}\partial^1_{z_2}...\partial^{N-3}_{z_{N-2}}\partial^{N-1}_{z_N}\partial^N_{z_{N-1}}(z_1^0 z_2^2...z_N^{2(N-1)})\ ,$$

but they are eliminated in the antisymmetrizing part of the derivatives. Because the sign of the derivative is the same as corresponding sign for the permutation, the antisymmetric derivative for $k=1$ is automatically of the form of Slater determinant.

We have shown that the diagonal part behaves in the antisymmetric derivative as Equation (B.8) claims. The Equation (B.17) gives us corresponding front coefficient for that part. The final result for the antisymmetric derivative of the diagonal part with $k=1$, is thus

$$\begin{aligned}
&A_{der,\text{diag}} = C_{N_{\text{diag}}}\prod_{i<j}^{N}(z_i - z_j)\ \text{, where} \\
&C_{N_{\text{diag}}} = (-1)^{\frac{N(N-1)}{2}}\frac{1}{N!}2^{N-1}(N-1)!\cdot\frac{1!}{1!}\cdot\frac{3!}{2!}\cdot ...\cdot\frac{(2N-5)!}{(N-2)!}\cdot\frac{(2N-3)!}{(N-1)!}\ .
\end{aligned} \tag{B.18}$$

In the Table B.1 coefficients calculated from the Equation (B.18), are presented. We have verified the values by computing the antisymmetric derivative for diagonal part as in Equation (B.16), and the results equal.

Next we should prove that the cross-term-sum D_{cross} behaves also as stated in (B.8) in the antisymmetric derivative. It will be a lot more difficult than proving corresponding equation for the diagonal part D_{diag}. This is due to the fact that there are $\binom{N!}{2}$ terms in the cross-term-sum. One observes that there is not a simple form for the result such as a product of simple terms depending on N, that would be multiplied with a factor 2^N. This can be seen by comparing coefficients for diagonal part and for cross-term part (Table B.2). From the table one can observe that the prime number factors in the

Table B.1: The contribution from diagonal-term-sum into the ground state wave function in two to seven particle cases. The results are calculated both from Equation (B.18), and for comparison, directly with Mathematica. In both cases, the results are the same.

N	$A_{der,\text{diag}}$
2	$-\prod_{i<j}^{2}(z_i - z_j)$
3	$-4\prod_{i<j}^{3}(z_i - z_j)$
4	$120\prod_{i<j}^{4}(z_i - z_j)$
5	$40320\prod_{i<j}^{5}(z_i - z_j)$
6	$-203212800\prod_{i<j}^{6}(z_i - z_j)$
7	$-19313344512000\prod_{i<j}^{7}(z_i - z_j)$

Table B.2: The contributions of diagonal-term-sum and cross term sum terms into factor C_N.

N	$C_{N,\text{diag}}$	$C_{N,\text{cross}}$
2	-1	-1
3	-2^2	$-2\cdot 3^2$
4	$2^3\cdot 3\cdot 5$	$2^2\cdot 523$
5	$2^7\cdot 3^2\cdot 5\cdot 7$	$2^4\cdot 3\cdot 7\cdot 8443$
6	$-2^{11}\cdot 3^4\cdot 5^2\cdot 7^2$	$-2^9\cdot 3^7\cdot 17\cdot 37\cdot 89$

coefficient for diagonal part are of order N as also (B.18) shows. Contradictory, the prime number factors in the coefficient for cross-term part are of much higher-order, and especially there is no simple dependence of N.

It seems to be impossible to have such a simple form to the coefficient of the cross term sum, as in the diagonal part $C_{N,\text{diag}}$. In spite of that it is possible to show that the cross term coefficient consists of sum of terms such like $C_{N,\text{diag}}$. First we notice that the number of terms in the crossterm sum D_{cross} can be halved by writing

$$\begin{aligned} D_{\text{cross}} &= 2 \sum_{\pi_v \neq \pi_w} z_1^{\pi_v(1)+\pi_w(1)} z_2^{\pi_v(2)+\pi_w(2)} ... z_N^{\pi_v(N)+\pi_w(N)} \\ &= 4 \sum_{\pi_v < \pi_w} \epsilon_{\pi_v}\epsilon_{\pi_w} z_1^{\pi_v(1)+\pi_w(1)} z_2^{\pi_v(2)+\pi_w(2)} ... z_N^{\pi_v(N)+\pi_w(N)} , \end{aligned} \tag{B.19}$$

where marking $\pi_v < \pi_w$ stands for summation over all permutations, where π_v is smaller than π_w. All one has to do is to invent a way to define the magnitude of certain permutation. This way of marking works only if every permutation has a magnitude. The solution is quite simple; we define the magnitude for every permutation so that we consider it as a number in $N+1$ number system. Then, permutation $(012...N)$ is the smallest in magnitude and permutation $(N...210)$ the greatest.

To conclude, we demonstrated how the composite fermion wave functions show the expansion related to the increase of angular momentum. It was done in a case of two-particle system and without using pair correlation function but my own method instead. We also tried to prove that the CF theory wave functions satisfy $\phi^{CF}_{\alpha,0,0} = \phi^{CF}_{0,\beta,1}$. We did not succeed in proving that generally, but it held true in every case we managed to compute.

Appendix C

Discussion of the solution of classical eigenenergies and eigenmodes

C.1 Three-particle case

Eigenfrequencies (eigenenergies) of a classical three-particle system with Coulombic inter-particle interaction are

$$\begin{aligned}
\omega_1 &= \omega_0 - \omega_{r_0} \\
\omega_2 &= \omega_0 + \omega_{r_0} \\
\omega_3 &= \sqrt[4]{3\omega_0^4 + 10\omega_0^2\omega_{r_0}^2 - \frac{7}{3}\omega_{r_0}^4 + \frac{R_3}{12S_3} - \frac{S_3}{12}} \\
\omega_4 &= \sqrt{3\omega_0^2 + \omega_{r_0}^2 - \omega_3^2} \\
\omega_5 &= \sqrt{3\omega_0^2 + \omega_{r_0}^2}\,,
\end{aligned} \tag{C.1}$$

where ω_0 stands for the strength of the confining harmonic potential, and ω_r is the rotation frequency.

Symbols R_3 and S_3 are on the form

$$\begin{aligned} R_3 =& -81\omega_0^8 - 3132\omega_0^6\omega_{r_0}^2 - 1638\omega_0^4\omega_{r_0}^4 + 708\omega_0^2\omega_{r_0}^6 + 47\omega_{r_0}^8 \\ S_3 =& \Big(-729\omega_0^{12} + 62694\omega_0^{10}\omega_{r_0}^2 + 234009\omega_0^8\omega_{r_0}^4 - 108\omega_0^6\omega_{r_0}^6 \\ & - 29079\omega_0^4\omega_{r_0}^8 - 7002\omega_0^2\omega_{r_0}^{10} + 2359\omega_{r_0}^{12} \\ & + i972\sqrt{6}\left(\omega_0^2 - \omega_{r_0}^2\right)^4 \sqrt{3\omega_0^2 - \omega_{r_0}^2}\left(\omega_0^2 + \omega_{r_0}^2\right)\omega_{r_0}\Big)^{\frac{1}{3}}. \end{aligned} \tag{C.2}$$

It is interesting to note that even though S_3 is complex, the eigenfrequencies ω_3 and ω_4 are real when $\omega_{r_0} \in [0, \omega_0]$.

Using molecular dynamics simulations, the eigenfrequencies can be solved from the velocity-velocity autocorrelation function. Figure C.1 shows that the eigenfrequencies of Eq. (C.1) correspond to those solved by computer simulation. Because simulation in this case represents an experiment (when one checks the correctness of the derived results), it is reasonable to assume that the eigenfrequencies are derived correctly. Mathematical forms for the corresponding eigenmodes are as follows

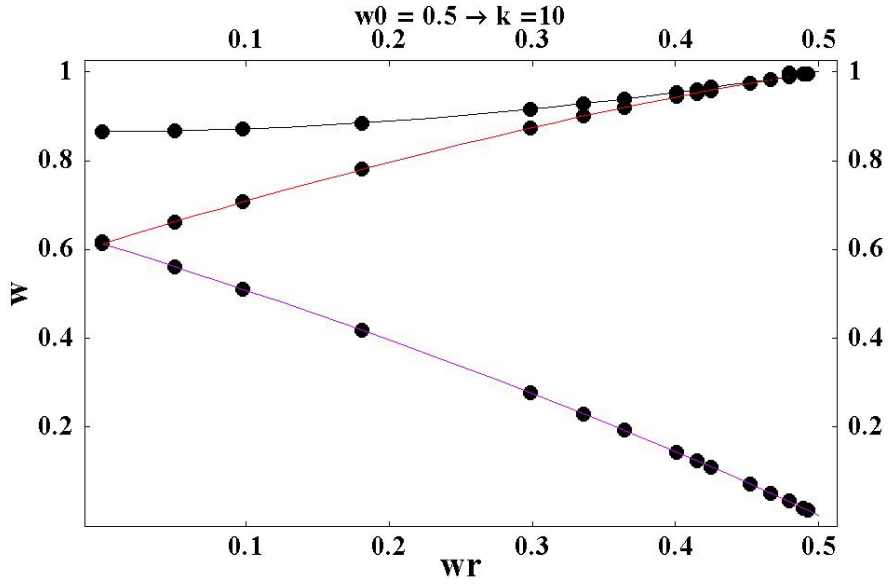

Figure C.1: In this figure eigenfrequencies presented in equation (C.1), are compared to those solved with computer simulation (black dots). One observes that the results are identical, which basically means that one may believe that eigenfrequencies (C.1) are correct. Black solid line stands for the "breathing" mode, and violet and red line represent eigenfrequencies ω_3 and ω_4, respectively.

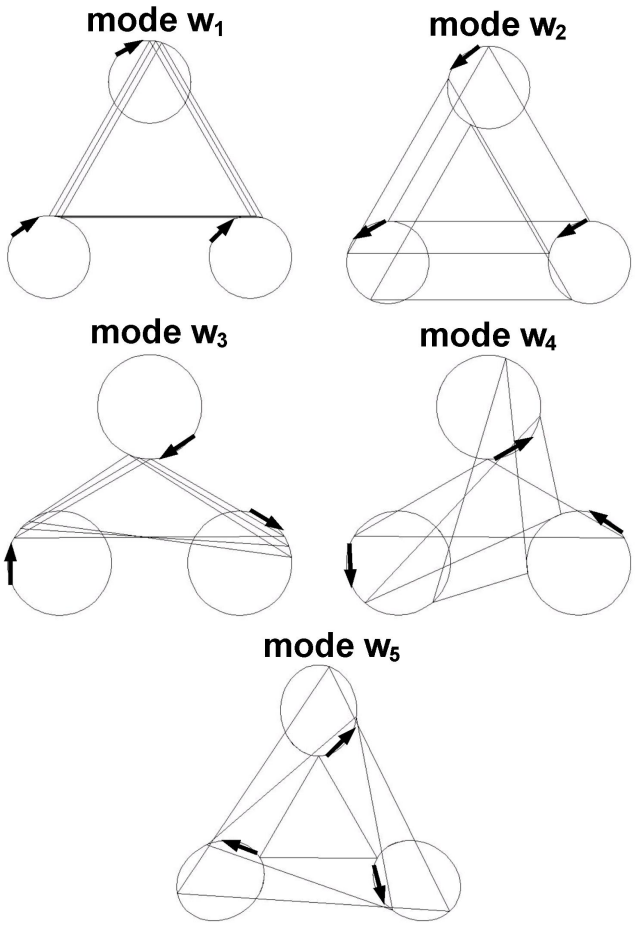

Figure C.2: The eigenfrequencies for three classical (charged) particles confined into a harmonic potential. In all cases the angular momentum is so that corresponding angular frequency $\omega_{r_0} = 0{,}4$. From the upper left onwards the modes are ω_1, ω_2, ω_3, ω_4 and ω_5, respectively.

$$
\begin{aligned}
\mathbf{X}_1 =& D_{\omega_1,1}(-i,-i,-i,1,1,1)e^{i\omega_1 t} + D_{\omega_1,2}(i,i,i,1,1,1)e^{-i\omega_1 t} \\
\mathbf{X}_2 =& D_{\omega_2,1}(i,i,i,1,1,1)e^{i\omega_2 t} + D_{\omega_2,2}(-i,-i,-i,1,1,1)e^{-i\omega_2 t} \\
\mathbf{X}_3 =& D_{\omega_3,1}(-\sqrt{3}+i,\sqrt{3}+i,-2i,-1-\sqrt{3}i,-1+\sqrt{3}i,2)e^{i\omega_3 t} \\
&+ D_{\omega_3,2}(-\sqrt{3}-i,\sqrt{3}-i,2i,-1+\sqrt{3}i,-1-\sqrt{3}i,2)e^{-i\omega_3 t} \\
\mathbf{X}_4 =& D_{\omega_4,1}(\sqrt{3}+i,-\sqrt{3}+i,-2i,1-\sqrt{3}i,1+\sqrt{3}i,-2)e^{i\omega_4 t} \\
&+ D_{\omega_4,2}(\sqrt{3}-i,-\sqrt{3}-i,2i,1+\sqrt{3}i,1-\sqrt{3}i,-2)e^{-i\omega_4 t} \\
\mathbf{X}_5 =& D_{\omega_5,1}\Big(3\sqrt{3}\omega_0^2 + 5\sqrt{3}\omega_{r_0}^2 - 4i\omega_{r_0}\omega_5, -8\sqrt{3}\omega_{r_0}^2 - 4i\omega_{r_0}\omega_5, \\
&- 3\sqrt{3}\omega_0^2 + 3\sqrt{3}\omega_{r_0}^2 + 8i\omega_{r_0}\omega_5, 3\omega_0^2 - 11\omega_{r_0}^2 - 4\sqrt{3}i\omega_{r_0}\omega_5, \\
&- 6\omega_0^2 - 2\omega_{r_0}^2 + 4\sqrt{3}i\omega_{r_0}\omega_5, 3\omega_0^2 + 13\omega_{r_0}^2\Big)e^{i\omega_5 t} \\
&+ D_{\omega_5,2}\Big(3\sqrt{3}\omega_0^2 + 5\sqrt{3}\omega_{r_0}^2 + 4i\omega_{r_0}\omega_5, -8\sqrt{3}\omega_{r_0}^2 + 4i\omega_{r_0}\omega_5, \\
&- 3\sqrt{3}\omega_0^2 + 3\sqrt{3}\omega_{r_0}^2 - 8i\omega_{r_0}\omega_5, 3\omega_0^2 - 11\omega_{r_0}^2 + 4\sqrt{3}i\omega_{r_0}\omega_5, \\
&- 6\omega_0^2 - 2\omega_{r_0}^2 - 4\sqrt{3}i\omega_{r_0}\omega_5, 3\omega_0^2 + 13\omega_{r_0}^2\Big)e^{-i\omega_5 t}\,.
\end{aligned}
\tag{C.3}
$$

For every eigenmode i, its j^{th} component is on the form

$$\begin{aligned}\mathbf{X}_{i,j} =& D_{\omega_i,1}(A+Bi)e^{i\omega_i t} + D_{\omega_i,2}(A-Bi)e^{-i\omega_i t} \\ =& A(D_{\omega_i,1}+D_{\omega_i,2})\cos\omega_i t - B(D_{\omega_i,1}+D_{\omega_i,2})\sin\omega_i t \\ &+ i\underbrace{\left(A(D_{\omega_i,1}-D_{\omega_i,2})\sin\omega_i t + B(D_{\omega_i,1}-D_{\omega_i,2})\cos\omega_i t\right)}_{=0 \Rightarrow D_{\omega_i,1}=D_{\omega_i,2}} \\ =& 2D_{i,1}(A\cos\omega_i t - B\sin\omega_i t)\,,\end{aligned} \tag{C.4}$$

where we have required that the eigenmode is real. Therefore, the (real and normalized) eigenmodes are

$$\begin{aligned}\mathbf{X}_1 =& \frac{1}{\sqrt{6}}(\sin\omega_1 t, \sin\omega_1 t, \sin\omega_1 t, \cos\omega_1 t, \cos\omega_1 t, \cos\omega_1 t) \\ \mathbf{X}_2 =& \frac{1}{\sqrt{6}}(-\sin\omega_2 t, -\sin\omega_2 t, -\sin\omega_2 t, \cos\omega_2 t, \cos\omega_2 t, \cos\omega_2 t) \\ \mathbf{X}_3 =& \frac{1}{\sqrt{12}}\Big(-\sqrt{3}\cos\omega_3 t - \sin\omega_3 t, \sqrt{3}\cos\omega_3 t - \sin\omega_3 t, 2\sin\omega_3 t, \\ & -\cos\omega_3 t + \sqrt{3}\sin\omega_3 t, -\cos\omega_3 t - \sqrt{3}\sin\omega_3 t, 2\cos\omega_3 t\Big) \\ \mathbf{X}_4 =& \frac{1}{\sqrt{12}}\Big(\sqrt{3}\cos\omega_4 t - \sin\omega_4 t, -\sqrt{3}\cos\omega_4 t - \sin\omega_4 t, 2\sin\omega_4 t, \\ & \cos\omega_4 t + \sqrt{3}\sin\omega_4 t, \cos\omega_4 t - \sqrt{3}\sin\omega_4 t, -2\cos\omega_4 t\Big) \\ \mathbf{X}_5 =& \frac{1}{16\sqrt{3}\omega_0^2}\Big((3\omega_0^2+5\omega_{r_0}^2)\sqrt{3}\cos\omega_5 t + 4\omega_{r_0}\omega_5\sin\omega_5 t, -8\sqrt{3}\omega_{r_0}^2\cos\omega_5 t \\ & + 4\omega_{r_0}\omega_5\sin\omega_5 t, (-3\omega_0^2+3\omega_{r_0}^2)\sqrt{3}\cos\omega_5 t - 8\omega_{r_0}\omega_5\sin\omega_5 t, \\ & (3\omega_0^2-11\omega_{r_0}^2)\cos\omega_5 t + 4\sqrt{3}\omega_{r_0}\omega_5\sin\omega_5 t, -(6\omega_0^2+2\omega_{r_0}^2)\cos\omega_5 t \\ & - 4\sqrt{3}\omega_{r_0}\omega_5\sin\omega_5 t, (3\omega_0^2+13\omega_{r_0}^2)\cos\omega_5 t\Big)\,.\end{aligned} \tag{C.5}$$

In Figure C.2 the time dependencies of the eigenmodes are presented. Angular momentum is set so that $\omega_{r_0} = \omega_0$. From the upper left onwards, the two first modes correspond to center of mass vibrations, where the particles rotate clockwise or counterclockwise on circular orbits around their equilibrium positions. Two following modes are the eigenmodes ω_3 and ω_4, respectively. The first of those rotates clockwise and the latter counterclockwise. The last mode is the "breathing" mode, and in that the particles rotate counterclockwise on their eclipse orbits.

The eigenmodes ω_3 and ω_4 are degenerate when the angular momentum equals zero. The degeneracy vanishes when the system starts to rotate. When one examines Figure C.2, the disappearing of the degenaracy seems to be understandable. In a rotating frame of reference the modes rotating clockwise vibrate slower and the frequency goes to zero, when $\omega_{r_0} = \omega_0$. Opposite to that, the eigenfrequencies of the counterclockwise modes increase when the angular momentum is increased, approaching to

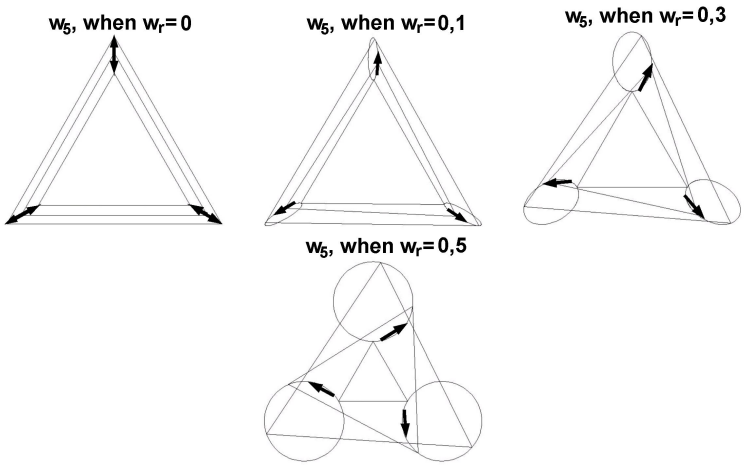

Figure C.3: "Breathing" mode is shown as a function of angular momentum.

$2\omega_0$. This phenomenon is demonstrated in Figure C.3, where the "breathing" mode is considered. From the figure one sees that at low angular momentum values the particles rotate on narrow eclipses and finally, with $\omega_5 = \omega_0$, the particles rotate on circular orbits. Note that the particle configuration is always an equilateral triangle.

C.2 Four-particle case

The eigenmodes of the four-particle case are

$$\begin{aligned}
\omega_1 &= \omega_0 - \omega_{r_0} \\
\omega_2 &= \omega_0 + \omega_{r_0} \\
\omega_3 &= \sqrt{\frac{3\omega_0^2}{2} + \frac{\omega_{r_0}^2}{2} - R_4} \\
\omega_4 &= S_4 - \omega_{r_0} \\
\omega_5 &= S_4 + \omega_{r_0} \\
\omega_6 &= \sqrt{\frac{3\omega_0^2}{2} + \frac{\omega_{r_0}^2}{2} + R_4} \\
\omega_7 &= \sqrt{3\omega_0^2 + \omega_{r_0}^2}\,,
\end{aligned} \tag{C.6}$$

where the coefficient R_4 and S_4 are

$$\begin{aligned}
R_4 =& \frac{1}{14}\Big(\left(1017 - 648\sqrt{2}\right)\omega_0^4 \\
& \left(1296\sqrt{2} - 858\right)\omega_0^2\omega_{r_0}^2 + \left(625 - 648\sqrt{2}\right)\omega_{r_0}^4 \Big)^{\frac{1}{2}} \\
S_4 =& \frac{\sqrt{7}}{7}\sqrt{\left(15 - 2\sqrt{2}\right)\omega_0^2 + \left(2\sqrt{2} - 8\right)\omega_{r_0}^2}\,.
\end{aligned} \tag{C.7}$$

As for three particles, one has to first check that the numerical values of the modes are correct. It is done on the same way as in the three-particle case, by comparing the results with computer simulation results. The results of the comparison are presented in Figure C.4. We notice that the solid line representing the energy of the mode ω_5 intersects with the lines of ω_6 and ω_7. It is an interesting result but unfortunately does not appear with low energy modes. If this phenomenon happened with low energy modes, it would have been seen in the low energy spectrum of a quantum dot.

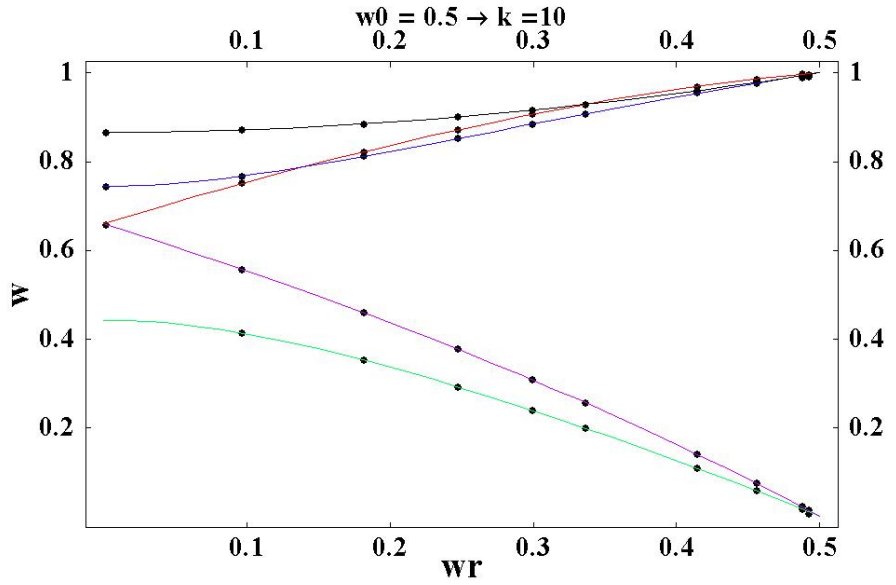

Figure C.4: Numerical values for the eigenmodes calculated with two methods: by linearization (C.6), and by solving them with computer simulation (corresponding to an experiment). One notes that the results are equal. The simulated results are shown as black dots, and the solid lines represent to the analytical results (C.6). Black solid line stands for the "breathing" mode, and violet, red, green and blue lines represent to modes $\omega_4, \omega_5, \omega_3$ and ω_6, respectively. An interesting fact is that when the angular momentum is increased, the mode ω_5 passes in energy first the mode ω_6 and finally the "breathing" mode ω_7. Unfortunately, this does not happen with low energy modes that contribute to the energy spectrum of a quantum dot.

The eigenvectors of the eigenfrequencies are solved as for four particles. We managed to solve analytical results for following modes: $\omega_1, \omega_2, \omega_4$ and ω_5, respectively, and they are

$$\begin{aligned}
\mathbf{X}_1 =& \frac{1}{2}(\sin\omega_1 t, \sin\omega_1 t, \sin\omega_1 t, \sin\omega_1 t, \\
& \cos\omega_1 t, \cos\omega_1 t, \cos\omega_1 t, \cos\omega_1 t) \\
\mathbf{X}_2 =& \frac{1}{2}(-\sin\omega_2 t, -\sin\omega_2 t, -\sin\omega_2 t, -\sin\omega_2 t, \\
& \cos\omega_2 t, \cos\omega_2 t, \cos\omega_2 t, \cos\omega_2 t) \\
\mathbf{X}_4 =& \frac{1}{2}(\sin\omega_4 t, -\sin\omega_4 t, \sin\omega_4 t, -\sin\omega_4 t, \\
& \cos\omega_4 t, -\cos\omega_4 t, \cos\omega_4 t, -\cos\omega_4 t) \\
\mathbf{X}_5 =& \frac{1}{2}(-\sin\omega_5 t, \sin\omega_5 t, -\sin\omega_5 t, \sin\omega_5 t, \\
& \cos\omega_5 t, -\cos\omega_5 t, \cos\omega_5 t, -\cos\omega_5 t)\ .
\end{aligned} \tag{C.8}$$

In the Figure C.5, the modes are shown in the case of $\omega_{r_0} = 0.4$. In all cases the time step between two different configurations, is equal. From upper left onwards the two first modes correspond to center of mass vibrations, and the following two to ω_4 and ω_5. One obtains from the figure that the paths of the modes ω_4 and ω_5 (as well as ω_1 and ω_2) are identical otherwise but the first rotates clockwise while the latter rotates counterclockwise.

We could not find the analytical solutions for the rest of the eigenmodes ω_3, ω_6 and ω_7. However, we managed to solve their orbits numerically, and in Figure C.6 the results are shown with few angular frequencies. The uppermost row of the figure represents the mode ω_3, the row on the middle represents the mode ω_6, and the lowest row mode ω_7 (i.e. "breathing" mode). From the figure one obtains that the paths of the modes ω_3 and ω_7 seem to be similar, and the only difference is that first rotates clockwise while the other rotates counterclockwise. One observes also that the particle configuration of the "breathing" mode is a square at every time step.

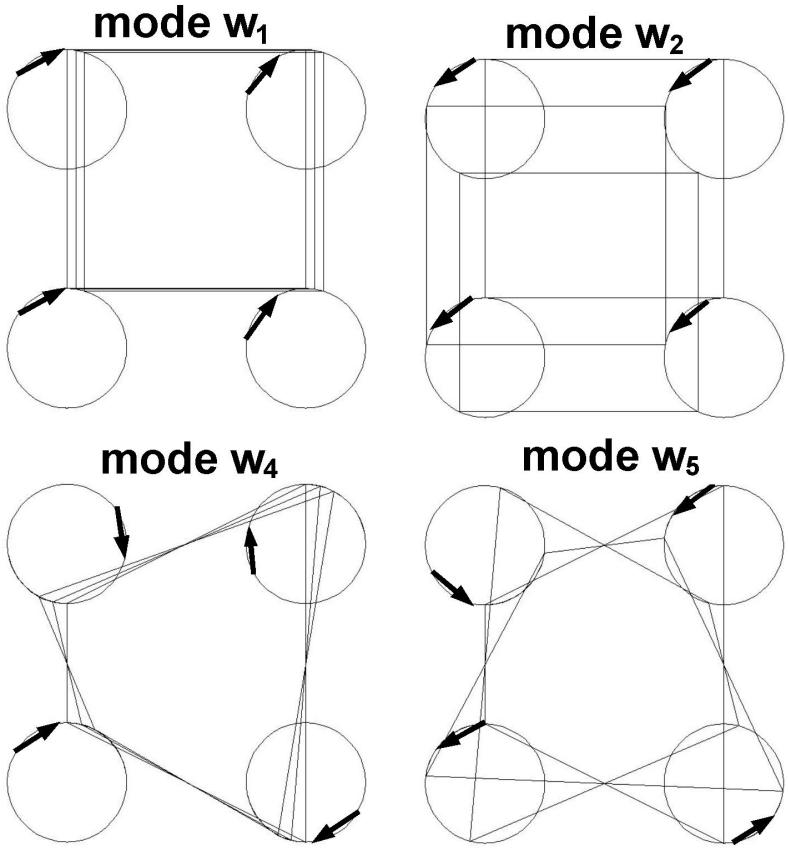

Figure C.5: Eigenmodes (C.8) are presented in this figure. From upper left onwards the two first modes correspond to ω_1 and ω_2, and the following two to ω_4 and ω_5. The rest of the modes are not shown in this figure, because We could not solve their analytical forms.

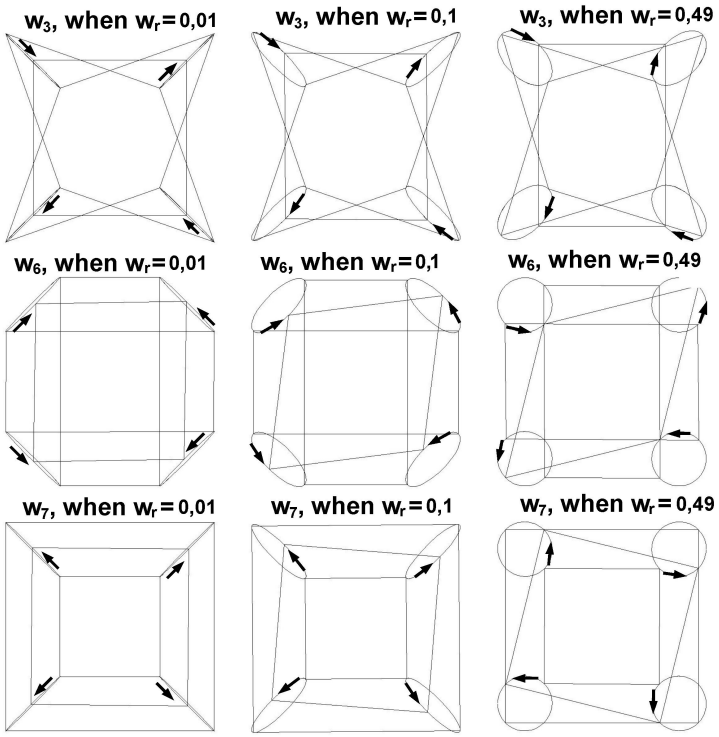

Figure C.6: The rest of the eigenmodes (ω_3, ω_6 and ω_7) of a four-particle system confined to a harmonic potential.

Although we could not actually solve the analytical solutions for the eigenmodes ω_3, ω_6 and ω_7, We managed to find out following analytical expressions to them

$$
\begin{aligned}
\mathbf{X}_3 =&\Big(-\frac{1}{\sqrt{8}}\cos\omega_3 t, T_{\omega_3,1}\cos\omega_3 t - T_{\omega_3,2}\sin\omega_3 t, \frac{1}{\sqrt{8}}\cos\omega_3 t, \\
&- T_{\omega_3,1}\cos\omega_3 t + T_{\omega_3,2}\sin\omega_3 t, -T_{\omega_3,1}\cos\omega_3 t + T_{\omega_3,2}\sin\omega_3 t, \\
&- \frac{1}{\sqrt{8}}\cos\omega_3 t, T_{\omega_3,1}\cos\omega_3 t - T_{\omega_3,2}\sin\omega_3 t, \frac{1}{\sqrt{8}}\cos\omega_3 t\Big) \\
\mathbf{X}_6 =&\Big(\frac{1}{\sqrt{8}}\cos\omega_6 t, T_{\omega_6,1}\cos\omega_6 t - T_{\omega_6,2}\sin\omega_6 t, -\frac{1}{\sqrt{8}}\cos\omega_6 t, \\
&- T_{\omega_6,1}\cos\omega_6 t + T_{\omega_6,2}\sin\omega_6 t, -T_{\omega_6,1}\cos\omega_6 t + T_{\omega_6,2}\sin\omega_6 t, \\
&\frac{1}{\sqrt{8}}\cos\omega_6 t, T_{\omega_6,1}\cos\omega_6 t - T_{\omega_6,2}\sin\omega_6 t, -\frac{1}{\sqrt{8}}\cos\omega_6 t\Big) \\
\mathbf{X}_7 =&\Big(-\frac{1}{\sqrt{8}}\cos\omega_7 t, -T_{\omega_7,1}\cos\omega_7 t - T_{\omega_7,2}\sin\omega_7 t, \frac{1}{\sqrt{8}}\cos\omega_7 t, \\
&T_{\omega_7,1}\cos\omega_7 t + T_{\omega_7,2}\sin\omega_7 t, -T_{\omega_7,1}\cos\omega_7 t - T_{\omega_7,2}\sin\omega_7 t, \\
&\frac{1}{\sqrt{8}}\cos\omega_7 t, T_{\omega_7,1}\cos\omega_7 t + T_{\omega_7,2}\sin\omega_7 t, -\frac{1}{\sqrt{8}}\cos\omega_7 t\Big)\,,
\end{aligned}
\tag{C.9}
$$

where some of the parameters seem to obey the following rules

$$\begin{aligned}
&\sqrt{T_{\omega_j,1}^2 + T_{\omega_j,2}^2} = \frac{1}{\sqrt{8}} \\
&T_{\omega_6,1}, T_{\omega_7,1} \to 0, \text{ when } \omega_{r_0} \to \omega_0 \\
&T_{\omega_6,2}, T_{\omega_7,2} \to \frac{1}{\sqrt{8}}, \text{ when } \omega_{r_0} \to \omega_0 \ .
\end{aligned} \tag{C.10}$$

The parameters $T_{\omega_3,1}$ and $T_{\omega_3,2}$ approach to some different values than 0 or $\frac{1}{\sqrt{8}}$.

To summarize, we observed that the energies of all modes rotating clockwise (counterclockwise) decrease (increase) as a function of ω_r. The most interesting results was that the energy of the mode ω_5 passes the energy of the modes ω_6 and ω_7. Unfortunately, these modes are not interesting for this work, because they do not contribute to the low energy spectrum of a quantum dot. Finally, we want to emphasize that the energy of the "breathing" mode was of the same form as in the case of three particles.

Bibliography

I J.-P. Nikkarila and M. Manninen, *Rotating electrons in quantum dots: Classical limit*, Solid State Commun. **141**, 209-213 (2007).

II M. Koskinen, S.M. Reimann, J.-P. Nikkarila and M. Manninen, *Spectral properties of rotating electrons in quantum dots and their relation to quantum Hall liquids*, J. Phys.: Condens. Matter, **19** 076211 (2007).

III J.-P. Nikkarila and M. Manninen, *Localization of particles in harmonic confinement: Effect of the interparticle interaction*, Phys. Rev. A **76**, 013622 (2007).

IV J.-P. Nikkarila, M. Koskinen, S.M. Reimann, and M. Manninen, *Magnetic phases of one-dimensional lattices with* 2 *to* 4 *fermions per site*, New J. Phys. **10**, (2008) 063013

V J.-P. Nikkarila, M. Koskinen, and M. Manninen, *Magnetism of quantum dot clusters: A Hubbard model study*, Eur. Phys. J. B **64**, 95-103 (2008)

[1] K. v. Klitzing, G. Dorda and M. Pepper, Phys. Rev. Lett. **45**, 494 (1980).

[2] Florian R. Ong, Olivier Bourgeois, Sergey E. Skipetrov, and Jacques Chaussy, Phys. Rev. B **74**, 140503 (2006).

[3] Richard E. Prange, Steven M. Girvin, *The Quantum Hall Effect* (2nd ed.) (Springer-Verlag New York Inc. 1990).

[4] B. Jeckelmann and B. Jeanneret, IEEE Trans Instrum. Meas. **46**, 276 (1997).

[5] Jeckelmann, B.; Rufenacht, A.; Jeanneret, B.; Overney, F.; Pierz, K.; von Campenhausen, A.; Hein, G., 2000 Conference, 521-522 (2000)

[6] For example, the finnish national laboratory (MIKES) realizes the standard for resistance with the help of the quantum Hall effect, *www.mikes.fi*

[7] H K Singh, and N D Kataria Florian, National Physical Laboratory *(of India)*, *Quantum Hall Effect as a resistance standard*

[8] D.C. Tsui, H.L. Störmer, A.C. Gossard, Physical Review Letters, **48**, 22 (1982).

[9] Ekimov, A.I., Onushchenko, A.A.: JETP Lett. **34**, 345 (1981)

[10] Efros, Al.L., Efros, A.L.: Fiz. Tekh. Poluprovodn., **16**, 1209 (1982)

[11] Brus, L.E.: J. Chem. Phys., **79**, 5566 (1983)

[12] Brus, L.E.: J. Chem. Phys., **80**, 4403 (1984)

[13] A.I. Ekimov, Al.L. Efros and A.A. Onushchenko, Solid State Commun., **56**, 921 (1985)

[14] P.A. Maksym, Phys. Rev. B **53**, 10871 (1996).

[15] P.A. Maksym, H. Imamura, G.P. Mallon, and A. Aoki, J. Phys. Cond. Mat. **12**, R299 (2000).

[16] S.M. Reimann, M. Koskinen, Y. Yu, and M. Manninen, New J. Phys., **8**, 59 (2006).

[17] W.A. de Heer, P. Milani, and A. Chatelain, Phys. Rev. Lett. **65**, 488 (1990)

[18] I. M. L. Billas, A. Chatelain, and W. A. de Heer, Science **265**, 1682 (1994)

[19] J. P. Bucher, D. C. Douglass, and L. A. Bloomfield, Phys. Rev. Lett. **66**, 3052 (1991)

[20] D. C. Douglass, A. J. Cox, J. P. Bucher, and L. A. Bloomfield, Phys. Rev. B **47**, 12 874 (1993).

[21] S. E. Apsel, J. W. Emmert, J. Deng, and L. A. Bloomfield, Phys. Rev. Lett. **76**, 1441 (1996)

[22] G.M. Pastor, R. Hirsch, and B. Mühlschleger, Phys. Rev. Lett. **72**, 3879 (1994).

[23] F. Lopez-Urias, G.M. Pastor, Phys. Rev. B **59** 5223 (1999).

[24] M. Koskinen, M. Manninen, and S.M. Reiman, Phys. Rev. Lett. **79**, 1389 (1997).

[25] S.M. Reimann and M. Manninen, Rev. Mod. Phys. **74**, 1283 (2002).

[26] R. Lo´pez-Sandoval, and G. M. Pastor Phys. Rev. B **67**, 035115 (2003)

[27] R. Lo´pez-Sandoval, and G. M. Pastor Phys. Rev. B **69**, 085101 (2004)

[28] H. Lee, J.A. Johnson, M.Y. He, J.S. Speck, and P.M. Petroff Appl. Phys. Lett. **78**, 105 (2001).

[29] M. Schmidbauer, S. Seydmohamadi, D. Grigoriev, Z.M. Wang, Y.I. Mazur, P. Schafer, M. Hanke, R. Kohler, and G.J. Salamo, Phys. Rev. Lett. **96**, 066108 (2006).

[30] S. Kohmoto, H. Nakamura, S. Nishikawa, and K. Asakawa, Physica E **13**, 1131 (2002).

[31] Köhl, M. & Esslinger, T., *Europhysics News* **37**, 18 (2006).

[32] Jaksch, D. & Zoller, P., *Annals of Physics* **315**, 52 (2005).

[33] M. Greiner, O. Mandel, T. Esslinger, T.W. Hänsch and I. Bloch, Nature **415**, 39 (2002).

[34] D.J. Han, S. Wolf, S. Oliver, C. McCormick, M. T. DePue, and D.S.Weiss, Phys. Rev. Lett. **85**, 724 (2000).

[35] A.J. Kerman, V. Vuletic, C. Chin, and S. Chu, Phys. Rev. Lett. **84**, 439 (2000).

[36] G. Modugno, F. Ferlaino, R. Heidemann, G. Roati, and M. Inguscio, Phys. Rev. A **68**, 011601 (2003).

[37] T. Rom, Th. Best, D. van Oosten, U. Schneider, S. Fölling, B. Paredes, and I. Bloch, Nature **444**, 733 (2006).

[38] J.K. Chin, D.E. Miller, Y. Liu, C. Stan, W. Setiawan, C. Sanner, K. Xu, and W. Ketterle, Nature **443**, 961 (2006).

[39] Feshbach, H., *Annals of Physics* **5**, 357 (1958).

[40] Inouye, S., *et al. Nature* **392**, 151 (1998).

[41] Courteille, Ph. *et al., Phys. Rev. Lett.* **81**, 69 (1998).

[42] Roberts, J. L. *et al., Phys. Rev. Lett.* **81**, 5109 (1998).

[43] Duine, R. A. & Stoof, H. T. C., *Physics Reports* **396**, 115 (2004)

[44] Theis, M., *Phys. Rev. Lett.* **93**, 123001 (2004)

[45] M. Koskinen, S.M. Reimann, and M. Manninen, Phys. Rev. Lett. **90**, 066802 (2003).

[46] K. Karkkainen, M. Koskinen, S.M. Reimann, and M. Manninen, Phys. Rev. B **72**, 165324 (2005).

[47] K. Kärkkäinen, M. Borgh, M. Manninen, and S.M. Reimann, New J. Phys. **9**, 33 (2007).

[48] K. Kärkkäinen, M. Borgh, M. Manninen, and S.M. Reimann, Eur. Phys. J D **43**, 225 (2007).

[49] P. Koskinen, L. Sapienza, and M. Manninen, Physica Scripta **68**, 74 (2003).

[50] J.Kolehmainen, S.M. Reimann, M. Koskinen, and M. Manninen, Eur. Phys. J. B **13**, 731 (2000).

[51] C. Yannouleas and U. Landman, Phys. Rev. Lett. **82**, 5325 (1999).

[52] M. Bayer, P. Hawrylak, K. Hinzer, S. Fafard, M. Korkusinski, Z.R. Wasilewski, O. Stern, and A. Forchel, Science **291**, 451 (2001).

[53] A. Harju, S. Siljamaki S, and R.M. Nieminen, Phys. Rev. Lett. **88**, 226804 (2002).

[54] F. Mireles, S.E. Ulloa, F. Rojas, and E. Cota, Appl. Phys. Lett. **88**, 093118 (2006).

[55] M. Scheibner, M. F. Doty, I. V. Ponomarev, A. S. Bracker, E. A. Stinaff, V. L. Korenev, T. L. Reinecke, and D. Gammon, Phys. Rev. B **75**, 245318 (2007).

[56] W. Zhang, T. Dong, and A.O. Govorov, Phys. Rev. B **76**, 075319 (2007).

[57] H. Chen, J. Wu, Z.Q. Li, and Y. Kawazoe, Phys. Rev. B **55**, 1578 (1997).

[58] M. Taut, Phys. Rev. B **62**, 8126 (2000).

[59] S.-J. Gu, R. Fan, and H.-Q. Lin, Phys. Rev. B **76**, 125107 (2007).

[60] G. Xianlong, M. Rizzi, Marco Polini, R. Fazio, M.P. Tosi, V.L. Campo, Jr., and K. Capelle, Phys. Rev. Lett. **98**, 030404 (2007).

[61] T. Koponen, J. Kinnunen, J.P. Martikainen, L.M. Jensen, P. Törmä, New. J. Phys. **8**, 179 (2006).

[62] T.K. Koponen, T. Paananen, J.P. Martikainen, and P. Törmä, Phys. Rev. Lett. **99** 120403 (2007).

[63] T. Paananen, T.K. Koponen, P. Törmä, and J.P. Martikainen *cond-mat/0801.1015*, (2008)

[64] J. Voit, Rep. Prog. Phys. **57**, 977 (1994).

[65] E.B. Kolomeisky, and J.P. Straley, Rev. Mod. Phys. **68**, 175 (1996).

[66] E.H. Lieb and F.Y. Wu, Phys. Rev. Lett. **20**, 1445 (1968).

[67] S. Viefers, P. Koskinen, P.S. Deo, and M. Manninen, Physica E **21**, 1 (2004).

[68] Csaba Toke, J. K. Jain, Phys. Rev. B, **76**, 081403(R) (2007).

[69] R. B. Laughlin, Phys. Rev. B, **23**, 5632 (1981).

[70] R. B. Laughlin, Phys. Rev. Lett., **50**, 1395 (1983).

[71] R. B. Laughlin, Phys. Rev. B, **27**, 3383 (1983).

[72] F. D. M. Haldane Phys. Rev. Lett., **51**, 605 (1983).

[73] B. I. Halperin Phys. Rev. Lett., **52**, 1583 (1984).

[74] R. Willett, J. P. Eisenstein, H. L. Störmer, D. C. Tsui, A. C. Gossard and J. H. English, Phys. Rev. Lett. **59**, 1776 (1987).

[75] J.K. Jain, Phys. Rev. Lett., **63**, 199 (1989).

[76] J.K. Jain, Phys. Rev. B **41**, 7653 (1990).

[77] J. K. Jain and T. Kawamura, Europhysics Letters, **29** (4), pp. 321-326 (1995).

[78] T. Chakraborty, *Quantum Dots: A Survey of the Properties of Artificial Atoms*, first edition (Elsevier 1999).

[79] S. M. Reimann and M. Manninen, Rev. Mod. Phys., **74** 1283 (2002).

[80] Stephen T. Thornton and Jerry B. Marion, (Thomson Brooks/Cole 2004).

[81] David J. Griffiths *Introduction to Quantum Mechanics* (Second Edition), (Pearson Education International 1995)

[82] V. Ruuska and M. Manninen, Phys. Rev. B **72**, 15 (2004).

[83] Murray R. Spiegel, John Liu, *Mathematical Handbook of Formulas and Tables*, 2nd edition (McGraw-Hill 1999).

[84] N.W. Ashcroft and N.D. Mermin, *Solid State Physics* (Saunders College, Philadelphia 1976).

[85] P.A. Maksym, Europhys. Lett. **31**, 405 (1995).

[86] M. Tinkham, *Group theory and quantum mechanics* (McGraw-Hill, New York 1964).

[87] F. Bolton and U. Rößler, Superlatt. Microstr. **13**, 139 (1993).

[88] V.M. Bedanov, and F.M. Peeters, Phys. Rev. B **49**, 2667 (1994).

[89] Angbo Fanga, Xuguang Chia and Ping Sheng, Solid State Commun. **142**, 551-555 (2007).

[90] Zhensheng Dai, Jia-Lin Zhu, Ning Yang, and Yuquan Wang, Phys. Rev. B **76**, 085308 (2007).

[91] Chuntai Shi, Gun Sang Jeon, and Jainendra K. Jain, Phys. Rev. B **75**, 165302 (2007).

[92] M. Manninen, Solid State Commun. **59**, 281 (1986).